TÉCNICO LISBOA

Analysis of the End Effects in a Spherical Induction Motor with Shell-Like Stator

André Filipe Mendonça Sá Roque

Thesis to obtain the Master of Science Degree in

Electrical and Computer Engineering

Supervisor(s): Prof. Paulo José da Costa Branco
Prof. João Filipe Pereira Fernandes

Examination Committee

Chairperson: **Prof. Rui Manuel Gameiro de Castro**
Supervisor: **Prof. Paulo José da Costa Branco**
Member of the Committee: **Prof. João José Esteves Santana**

November 2016

Acknowledgments

Um grande agradecimento aos meus colegas, sem os quais terminar o curso seria uma tarefa de impossível realização. A partilha dos bons e maus momentos e saber que ao meu lado estavam pessoas a passar pelo mesmo que eu tornou tudo mais fácil. Laços fortes foram criados sem os quais fazer este percurso teria muito menos significado do que agora.

Outro grande agradecimento ao professor João Fernandes, sem o qual a realização desta tese seria impossível. Principalmente na fase inicial, onde necessitei de maior ajuda, mostrou-se sempre disponível e com vontade de ajudar. Como não podia deixar de ser, um agradecimento também ao professor Paulo Branco, que me aceitou como aluno de mestrado e mostrou disponibilidade e empenho para se certificar do meu sucesso.

Por fim, um enorme agradecimento à minha família: pai, mãe, irmã, tios, primos e avó, com especial carinho ao meu primo cuja coragem, força e vontade de viver também me impeliram nesta etapa da minha vida, e continuará a ser fonte de inspiração para mim para o resto da minha vida. A minha família deu-me todas e mais algumas ferramentas que necessitei para chegar aqui, pelo que a eles estarei eternamente grato.

Resumo

O presente trabalho visou estabelecer a equação geral e encontrar uma solução particular do campo magnético dentro do entreferro de uma máquina de estator em concha e de rotor esférico. Na geometria desta máquina, existe uma descontinuidade do núcleo de ferro do estator, o que gera um perfil complicado para o campo magnético dentro do entreferro além da típica onda viajante. A este fenómeno atribui-se o nome de efeitos de borda. Para o efeito, utilizou-se como base estudos prévios feitos em efeitos de borda de motores lineares de indução através da Teoria de Campos, que partilham com este motor de rotor esférico a sua descontinuidade do núcleo de ferro do estator. Desta forma, procurou-se estabelecer uma ligação entre os efeitos de borda nas duas geometrias, tendo em conta que a análise ao motor esférico foi realizada em coordenadas cilíndricas, enquanto que nos motores lineares foi realizada em coordenadas Cartesianas. Estabeleceu-se um modelo para o campo magnético no entreferro e os seus parâmetros foram avaliados para várias configurações do motor, como vários tamanhos de entreferro, resistividades do condutor secundário, raios do rotor e frequências da rede. Obtiveram-se curvas de força para o motor e foi estabelecida a influência dos efeitos de borda no desempenho do motor sob várias condições, fazendo a distinção entre motores de alta velocidade e de baixa velocidade, cujos desempenhos são influenciados de forma diferente pelos efeitos de borda. Com base na variação dos parâmetros do modelo para várias configurações do motor, foi possível encontrar formas de diminuir a influência dos efeitos de borda no desempenho do motor.

Palavras-chave: Efeitos de Borda, Rotor Esférico, Motor de Indução, Estator em Concha, Campo Magnético

Abstract

This study aims to establish the general equation and find a particular solution to the magnetic field inside the air gap of a shell-like stator induction motor with spherical rotor. In this machine's geometry, a discontinuity of the stator iron core exists, creating a complex profile for the magnetic field inside the air gap, besides the travelling wave typically found. This phenomenon is called the end effects. In order to study these effects, previous studies of end effects in linear induction motors with Field Theory were used as a basis, whose geometry also shares the stator iron core discontinuity. Hence, a link between the end effects of the two geometries was sought, keeping in mind that the analysis for the spherical rotor was made in cylindrical coordinates, while Cartesian coordinates were used for the linear motor. A model was found for the magnetic field inside the air gap, and its parameters were tested for various motors configurations, such as varying air gaps, secondary sheet resistivity, rotor radiuses and power supply frequencies. Thrust curves were obtained and the impact of the end effects on motor performance was found, making a distinction between high speed and low speed motors, whose motor performance impact due to the end effect varies differently. It was possible to find ways to minimize the impact of the end effect on motor's performance from the variation of the model's parameters with various motor configurations.

Keywords: End Effects, Spherical Rotor, Induction Motor, Shell-Like Stator, Magnetic Field

Contents

List of Tables

List of Figures

Nomenclature

Greek symbols

α_1 Entry end effect penetration angle.

α_2 Exit end effect penetration angle.

β Stator angle in the θ coordinate.

ϵ Electromotive force.

μ_0 Air magnetic permeability.

ω Power supply angular frequency.

ω_e Angular speed of end effect waves.

ω_r Angular motor speed.

ω_s Angular synchronous speed.

ϕ Magnetic flux.

ρ Secondary sheet resistivity.

ρ_s Equivalent secondary sheet resistivity.

Roman symbols

B Magnetic field.

A Magnetic potential vector.

B_1 Amplitude of entry end effect wave.

B_2 Amplitude of exit end effect wave.

B_M Maximum amplitude of B_s.

B_s Amplitude of travelling wave.

B_{si} Amplitude of the magnetic field created by the induced currents.

d_r Secondary conductive sheet width.

d_s Primary conductive sheet width.

E Electric field.

g Air gap length.

H Magnetic field strength.

J_1 Equivalent amplitude of primary current density wave.

j_1 Primary current density.

j_2 Secondary current density.

J_M Amplitude of primary current density wave.

k Number of pair-poles.

k_e Equivalent number of pair-poles for end effect waves.

r Radius.

r_r Rotor radius.

r_s Stator radius.

s Slip.

v Linear velocity.

Chapter 1

Introduction

The end effects have been subject of study ever since the development of linear induction motors. Various authors have reported the effects over the years, and experiments were first conducted in Japan [1]. These effects are often divided in two categories [2]: longitudinal end effects and transverse end effects.

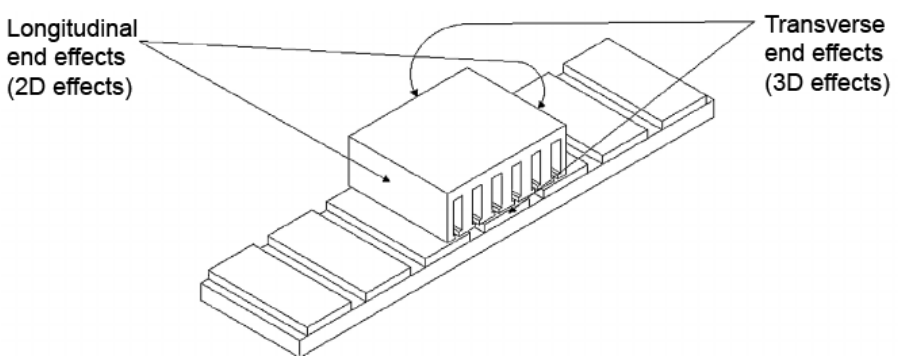

Figure 1.1: Longitudinal and transverse end effects representation [3].

The longitudinal end effects occur due to the discontinuity of the primary iron core, that is to say, the stator, in the direction of the movement of the motor, creating a turbulent magnetic field inside the air gap. These end effects are also divided in two categories: static and dynamic. The static end effects occur independently of the speed of the motor, and are influenced only by the geometry of the motor, namely, the primary windings distribution. The dynamic end effects are dependent on the motor speed, being more prevalent as the motor speed increases. Both these effects often

suffice in representing accurately the end effects of the linear induction motor.

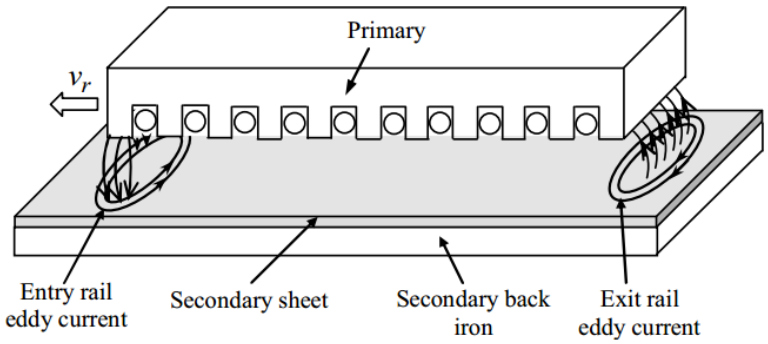

Figure 1.2: Longitudinal end effects representation [4].

The transverse end effects also occur due to the discontinuity of the primary iron core. Because the current pattern in the secondary is circular, a component of this current in the axis of the movement of the machine exists. This component does not contribute to the actual movement of the motor, since it is parallel to it, as shown in figure 1.3. Therefore, this current will create a magnetic field which will only oppose the magnetic field created by the primary, reducing performance. The path which this current exists is called the return path [5], as its only purpose is to close the lines of current in the secondary. These effects can often be disregarded, except in the case of very large air gaps.

1.1 Static End Effects

The static end effects can be explained through the magnetic circuit of the linear induction motor [6]. Because this magnetic circuit has a beginning and an end, the primary windings may be impossible to be placed symmetrically, as shown in figure 1.4. In this situation, the linear induction motor is said to have half-filled end slots.

This asymmetry in the windings provokes an unbalance on the primary currents [7]. This is evident when the Fortescue Transform is applied in figure 1.5, where it is possible to see not only a direct component but also an inverse and homopolar components of the current. This effect is called the static end effects.

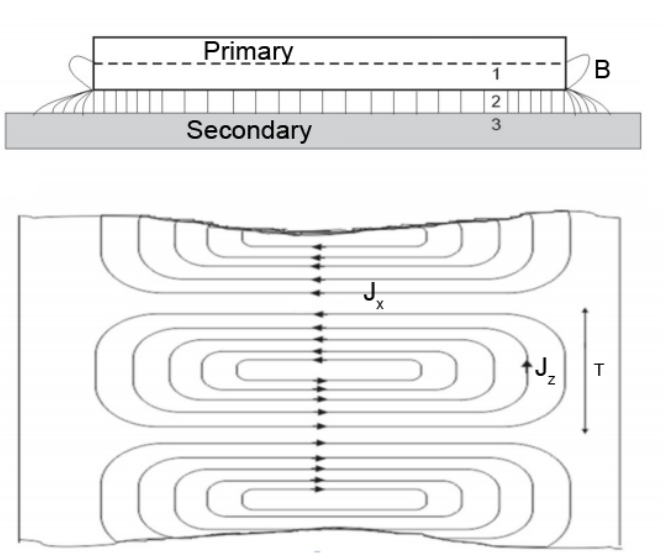

Figure 1.3: Transverse end effects representation [2].

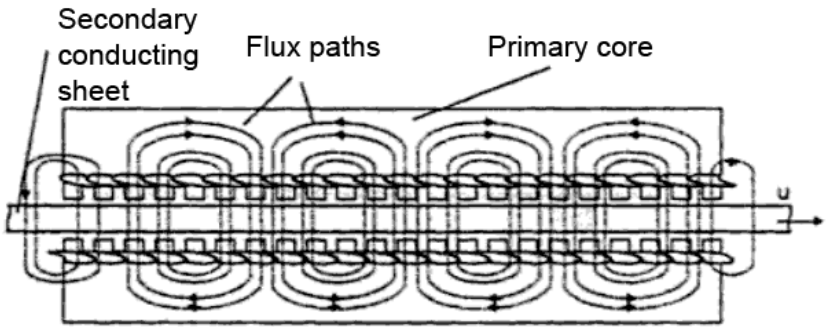

Figure 1.4: Half-filled end slots in a linear induction motor [6].

The inverse component in particular impacts negatively the motor performance. An oscillating force appears caused by this component, which is proportional to its amplitude. Another effect of these end effects appear under the form of additional Joule losses, which appear in both the primary windings and secondary conducting sheet.

These effects are often disregarded, and can be so in linear induction motors with number of poles greater than 6 [8].

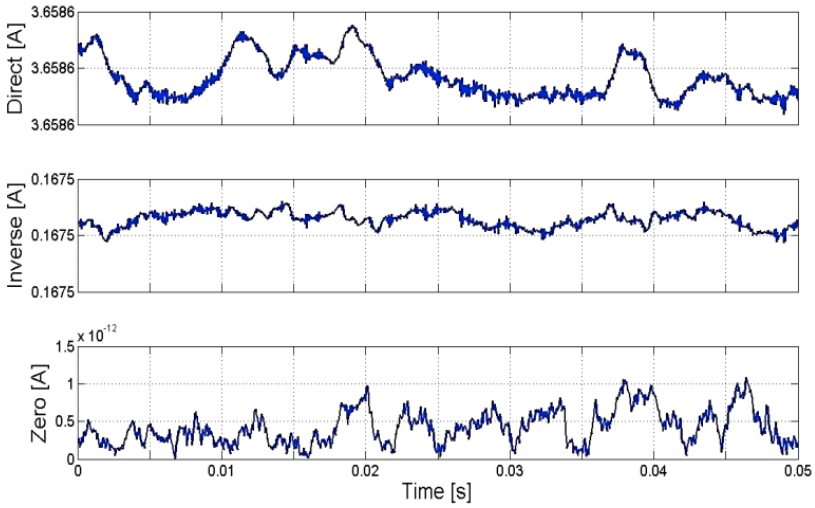

Figure 1.5: Direct, inverse and homopolar components of current in a linear induction motor [6].

1.2 Dynamic End Effects

The dynamic end effects occur as soon as the motor acquires speed [9]. To understand this phenomenon, a graphical explanation is required.

Considering a small domain in the secondary not under the influence of the primary, that is to say, away from the air gap, it is reasonable to say that both the magnetic field and current in this domain is zero. As this domain approaches the entry of the air gap, a sudden variation of magnetic field is verified, being provided by the primary. The secondary will respond opposing this sudden variation of magnetic field in this domain. Therefore, as this domain in the secondary starts to enter the air gap, instead of instantaneously raising its magnetic field to the one seen in the air gap, a damped increase of the magnetic field in this domain is seen. As will be seen further ahead, this damping has a time constant that is related to the characteristics of the iron in the secondary, in order to satisfy the continuity of the magnetic field along every domain of the secondary.

At the exit end, the opposite effect occurs. If the air gap is long enough, near the exit, there is no more damping of the magnetic field in the domain considered. Therefore, up until the end of the air gap, the magnetic field in this domain should have

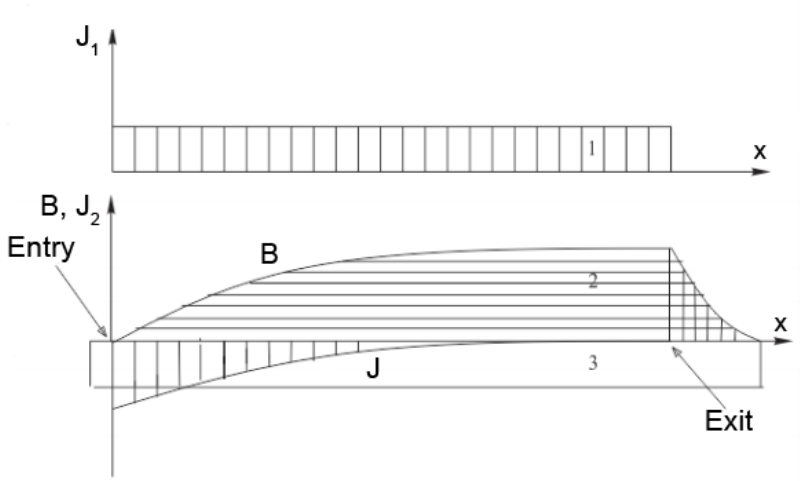

Figure 1.6: Dynamic end effects representation - primary current density J_1 and corresponding secondary current density J_2 and magnetic field in the air gap [2].

stabilised. As this domain exits the air gap, there is once again a sudden variation of the magnetic field and induced current, because it is no longer under the influence of the primary. This time, however, the domain will try to maintain its continuity by having a damped decrease of the magnetic field outside the air gap, creating a ”tail” as if it were of magnetic field. This damping's time constant is different from the first damping, as it is no longer under the primary ferromagnetic core.

1.3 Spherical Rotor Motor

The induction motor with spherical rotor and shell-like stator is proposed by this work's supervisor [10]. The functioning of the motor is based on the typical rotary induction motors with cylindrical rotors. However, by creating a spherical rotor and superposing two perpendicular primary windings, it is possible to control the rotor's motion in two axis, creating an omnidirectional machine. Because there is always a need to attach an axle to the rotor, in order to retrieve the mechanical energy related to the rotation of the rotor, applications for the spherical rotor induction motor are generally limited to certain degrees in each axis, as shown in figure 1.7.

The shell-like stator serves the purpose of inducing currents in the rotor's conduc-

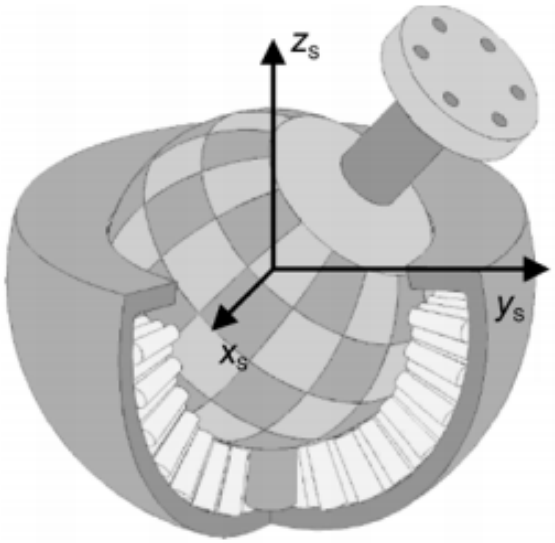

Figure 1.7: Spherical rotor visualization as per [11].

tive sheet, creating thrust and hence motion. A fully enclosed shell would have the best performance, as more current would be fed into the stator and hence to the rotor. However, it would also inhibit the degree in each of the two axis in which the rotor can rotate freely. Therefore, fully enclosed stators have little applications. This poses problems very closely related to the linear induction motor, as there is now a discontinuity of ferromagnetic material in the direction of motor of the rotor. This material discontinuity also causes a magnetic flux discontinuity in the air gap, called the end effect, which will affect motor performance.

1.4 Motivation

If applications of the spherical induction motor with shell-like stator are to be made, then there is a need to understand how its atypical geometry affects motor performance, and how heavily. Furthermore, a basis can be laid out for future analysis of similar geometries, as has been done in this very work with regards to the linear induction motor. A simple algorithm can be made which, given as input the motor's geometrical properties, can calculate how much influence the end effects will have, making it possible to

optimise motors in terms of their physical properties.

1.5 Objectives

Create a model that translates the magnetic field in the air gap of an induction machine with spherical rotor and shell-like stator, taking into account the end effects. This model should be independent of the geometrical properties of the motor, such as stator angle, as well as the electrical properties, such as number of pole-pair and primary windings distribution. Analyse the influence of the end effects in the machine's throughput, such as thrust, and discover the impact of different motor properties in the end effects.

1.6 Thesis Outline

In chapter 2, a brief summary how some of the mathematical tools needed will be used in this work, such as the definition of the coordinate system. In chapter 3, previous studies of linear induction motors and their end effects are analysed, in order to better understand the phenomenon of end effects in similar existing motors. A proposed model, based on the existing work, will be introduced in chapter 4, and analysis of its parameters will be made in chapter 5. Finally, the full magnetic field results can be found in chapter 6, which will provide comparison between the proposed model and simulations made in a Finite Element Analysis software. Lastly, conclusions will be taken in chapter 7.

Chapter 2

Fundamental Concepts

In order to understand the analysis made throughout this work, some basic concepts related to geometry and electromagnetism are needed. In this chapter, a simple explanation of these concepts is made, with emphasis on its implications in this work, in order to provide the reader some physical and mathematical background.

2.1 Cylindrical Coordinates

The cylindrical coordinate system used in this work with the convention (r, θ, z) describes a three-dimensional space as seen in figure 2.1 (a). Further in this work, some analogies will be made with the linear induction motor, which is described in Cartesian coordinates. Therefore, it is necessary to note the transformations between these coordinate systems. If a plane in cylindrical coordinates is considered with constant z, as if the spherical rotor machine was sliced, the machine would be represented as in figure 2.1 (b). In this simplified geometry, a few elements can be easily distinguished, enabling the transformation between Cartesian and cylindrical coordinates, as per table 2.1.

The curl operator in cylindrical coordinates, for a generic entity A, is given by equation 2.1. The cross product is given by the equations in 2.2, noting that $\vec{A} \times \vec{B} = -\vec{B} \times \vec{A}$.

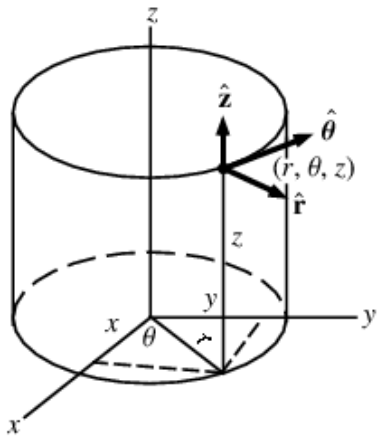

(a) Cylindrical coordinates system

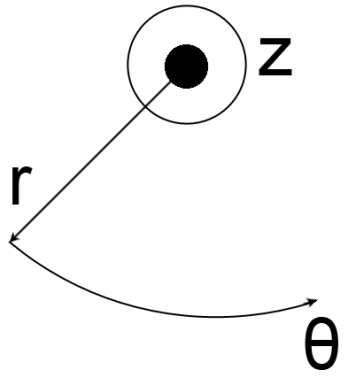

(b) Constant z plane in cylindrical coordinates.

Figure 2.1: Cylindrical coordinates

$$\nabla \times \mathbf{A} = \Big(\frac{1}{r}\frac{\partial A_z}{\partial \theta} - \frac{\partial A_\theta}{\partial z}\Big)\hat{\mathbf{r}} + \Big(\frac{\partial A_r}{\partial z} - \frac{\partial A_z}{\partial r}\Big)\hat{\boldsymbol{\theta}} + \frac{1}{r}\Big[\frac{\partial (rA_\theta)}{\partial r} - \frac{\partial A_r}{\partial \theta}\Big]\hat{\mathbf{z}} \tag{2.1}$$

$$\hat{\mathbf{r}} \times \hat{\boldsymbol{\theta}} = \hat{\mathbf{z}} \tag{2.2a}$$

$$\hat{\boldsymbol{\theta}} \times \hat{\mathbf{z}} = \hat{\mathbf{r}} \tag{2.2b}$$

$$\hat{\mathbf{z}} \times \hat{\mathbf{r}} = \hat{\boldsymbol{\theta}} \tag{2.2c}$$

It is now easy to link the two coordinate systems. For example, in this constant z height plane, in the Cartesian coordinates, a line element is $dx\hat{\mathbf{x}}$, which corresponds to, in the cylindrical coordinates with also constant z height plane, $rd\theta\hat{\boldsymbol{\theta}}$. This will be crucial when comparing literature regarding analysis of the linear induction motor in Cartesian coordinates with the spherical rotor machine's geometry.

Element	Cartesian Coordinates	Cylindrical Coordinates
Line	$dx\hat{\mathbf{x}}, dy\hat{\mathbf{y}}$	$rd\theta\hat{\boldsymbol{\theta}}, dr\hat{\mathbf{r}}$
Surface	$dxdy$	$rdrd\theta$
Volume	$dxdydz$	$rdrd\theta dz$

Table 2.1: Various elements expressed in Cartesian and Cylindrical coordinates.

2.2 Ampère's Law

The relationship between magnetic field and current can be described in most cases through the original Ampère's Law. The law may be expressed in either integral or differential form, through the Stoke's theorem.

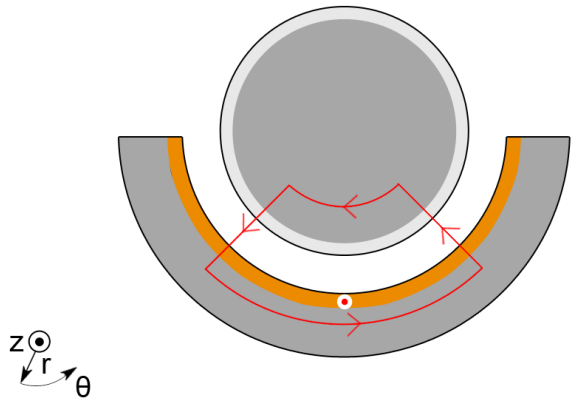

Figure 2.2: Application of Ampère's law in cylindrical coordinates.

The law states that the magnetic field around a closed surface, that is to say, the line integral, is equal to the current enclosed within that closed surface, the surface integral. This total current may also be expressed in terms of $j[A/m]$, the current density.

$$\oint_C \mathbf{H} dl = \iint_S \mathbf{j} dS \tag{2.3a}$$

$$\nabla \times \mathbf{H} = \mathbf{j} \tag{2.3b}$$

2.3 Gauss's Law for Magnetism

As in the case of Ampère's Circuital Law, Gauss's Law is one of Maxwell's equations for electrodynamics. The law, in its integral form, states that the magnetic flux within a closed surface is zero, that is to say, every line of magnetic flux that enters the surface also must exit through it.

$$\oiint_S \mathbf{B} dS = 0 \tag{2.4a}$$

$$\nabla \cdot \mathbf{B} = 0 \tag{2.4b}$$

This generally corresponds to the conservation of flux, which often is used as a boundary condition in many analysis. The relationship between magnetic flux and magnetic field is given by equation 2.5.

$$\phi = \iint_S \mathbf{B} dS \tag{2.5}$$

2.4 Electromotive Force and Lorentz's Force

The Electromotive Force results from the relative motion of a magnetic field and a conductor. In the case of an electrical machine, there is a magnetic field created by the primary passing through the secondary windings, therefore creating an electromotive force at its terminals. The current density in the secondary surface can therefore be represented in terms of the electromotive force, using Ohm's law and the secondary conductor resistivity.

$$\boldsymbol{\epsilon} = \rho \mathbf{j} \tag{2.6}$$

Lorentz's force states that there are two components of force in between a conductor and a magnetic field. One is the motional electromotive force, resulting from the movement of the conductor through a magnetic field. The other component is due to variation of the magnetic field, as per Faraday's law of induction in equation 2.7.

$$\boldsymbol{\epsilon} = -\frac{\partial \phi}{\partial t} \tag{2.7}$$

Both these components exist in electrical machines, as there is both a movement of the conductors in the rotor relative to the windings in the stator and a variation of the magnetic field due to the AC nature of the primary currents.

$$\boldsymbol{\epsilon} = \mathbf{E} + \mathbf{v} \times \mathbf{B} \tag{2.8a}$$

$$\mathbf{j} = \frac{1}{\rho}\big(\mathbf{E} + \mathbf{v} \times \mathbf{B}\big) \tag{2.8b}$$

2.5 Magnetic Vector Potential

The magnetic vector potential holds only a mathematical meaning, representing no physical entity. However, it is a very useful tool when analysis is made through the field theory. Further in this work, some relations between the magnetic vector potential and electrical and magnetic field are needed, which are here noted for the sake of clarity, as well as their relationship in cylindrical coordinates.

$$\mathbf{E} = -\frac{\partial \mathbf{A}}{\partial t} \tag{2.9a}$$

$$\frac{\partial \mathbf{A}}{\partial \theta} = r\mathbf{B} \tag{2.9b}$$

Chapter 3

Background

3.1 Linear Induction Motor Analysis

As already mentioned, extensive work on the analysis of end effects on linear induction motors has already been made. Several approaches have been taken in order to describe the influence of the phenomenon in motor performance. Some of these approaches will be presented, making an analogy with the spherical rotor machine.

3.1.1 Field Theory Analysis

Analysis on end effects is mostly done through Field Theory [1], [5], [12]. The magnetic circuit can be analysed through Ampère's Law and Electromotive Force, resulting in a differential equation for the magnetic field $\mathbf{B}$ inside the air gap.

Many approaches may be taken. The simplest is based on the assumption that the magnetic field inside the air gap is constant along the y coordinate, as per figure 3.1. Therefore, only a solution for $\mathbf{B_y}$ is to be found, which will be a function of x. This is called the one-dimensional model, which will be the one which this works delves into. For the one-dimensional approach, there are still many different considerations that can be taken into account. It is possible to create a second, third or even fourth order system [5].

The second order system is a simple application of both Ampère's Law and Electro-

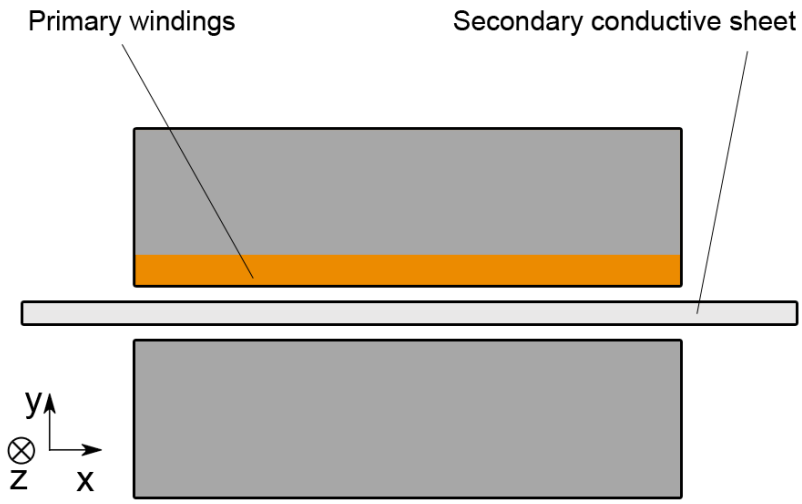

Figure 3.1: One-dimensional model for the linear induction motor.

motive Force in a small domain, while making no extra considerations. Equation 2.8b is inserted into equation 2.3b, resulting in a second order differential equation. Therefore, two roots exist for the transient term, or rather, the total solution is the superposition of two transient magnetic fields plus the steady state solution. These two transient magnetic fields, which will be studied in detail further ahead, are related to the necessity of continuity of magnetic flux in the extremities of the primary iron core, both entry and exit ends. The amplitudes of these transient waves can only be obtained through a set of boundary conditions, defined according to the geometry considered.

One boundary condition often used is the flux conservation, meaning that the steady state magnetic field solution, that is to say, the travelling wave created by the primary current density, and the transient magnetic fields, along the air gap length, must add up to zero. Another simple boundary condition is to consider that, outside the air gap, the secondary current density is zero, or in other words, that no magnetic field exists outside the air gap. As will be seen, this second condition might be too simplistic, and can be corrected by considering that there is magnetic field at a small distance outside the air gap.

The third order system considers the existence of return paths in the secondary sheet. These paths exist because the current in the secondary sheet is circular and,

therefore, has to close itself, as per figure 1.3. The currents that exist in this return path are parallel to the motion of the motor. Therefore, they do not contribute to the movement of the motor, and can be regarded as a purely Ohm loss in the secondary sheet. This affects the Electromotive Force, which now has to account for a loss of secondary current, due to the return paths. This results in a third order differential equation for the magnetic field inside the air gap. Three roots exist as a solution for the transient term. Two of them are essentially the same as the ones obtained in the second order system. The last term represents a constant magnetic field, therefore being present all through the air gap length and at any motor speed. This constant should not be confused with the static end effect referenced above, which is a different phenomenon that cannot be obtained through this kind of analysis.

The fourth order system considers not only the return path, in which the third order system is built, but also the a non infinite iron core permeability μ. The resulting fourth order differential equation, for very big μ, is the same as the third order differential equation. Four transient magnetic fields exist: two are again similar to the ones obtained in the second order system. The other two are both very close to the third root found in the third order system, that is, a constant term, and are almost equal and of opposite sign.

Another possible approach is to consider that there is in fact variation of the magnetic field in the y direction. Therefore, a solution for both B_x and B_y is to be found. This is called the two-dimensional analysis, which will result in two differential equations for each coordinate. The resulting solutions are both complex in form and difficult to interpret physically, involving hyperbolic functions. The same occurs with the boundary conditions and their results.

While the two-dimensional model is unquestionably more complete, it is also of much higher analytical complexity. For small air gaps and non-magnetic secondary sheets, the one-dimensional model will suffice in representing the magnetic field inside the air gap [1].

3.1.2 Equivalent Circuit

The analysis [9] is made considering the traditional rotary induction motor's equivalent model. When considering the end effect, it is explained that from the standpoint of view of the rotor, as the primary moves, the secondary's material is being continuously replaced by new material. This new material will oppose a sudden change in the magnetic flux, creating a gradual build up of magnetic field in the air gap, as explained above in the dynamic end effects section 1.2. This will affect the motor's performance, since the magnetic field in the air gap will not just be a travelling wave with constant amplitude. In order to obtain an equivalent circuit for a linear induction, this effect has to be added to the traditional equivalent circuit for induction motors.

If the primary is DC supplied, then a stationary flux wave can be obtained in the air gap if the secondary conducting sheet is removed. At time $t = 0$, if the conducting sheet is suddenly introduced, the magnetic flux in the air gap will display the build up mechanism, as seen in figure 3.2

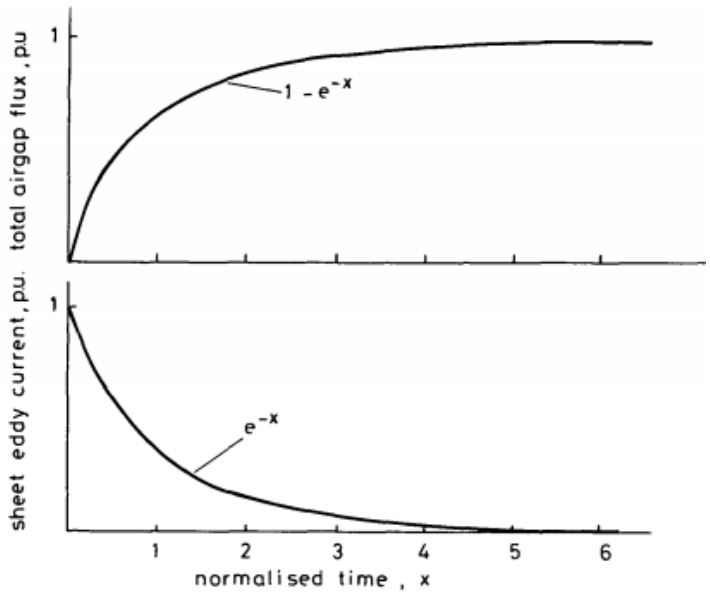

Figure 3.2: Build up mechanism of the magnetic field in the entry of the air gap [9].

The build up time depends on the secondary sheet's leakage time constant, $\frac{L_{2,1}}{R_{2,1}}$, as well as the magnetising time constant, $\frac{L_m}{R_{21}}$. Therefore, the total time constant is given by equation 3.1, where $L_{2,1}$ is the secondary leakage inductance referred to the primary,

$R_{2,1}$ is the secondary resistance referred to the primary and L_m is the magnetising inductance.

$$T_2 = \frac{L_{2,1} + L_m}{R_{2,1}} \tag{3.1}$$

It must also be noted that the primary magnetising current I_m represents the magnetomotive force per unit of length of motor, which gives rise to the air gap flux. As the primary winding turns per unit length of motor is fixed, the primary magnetising current I_m may be used to represent the magnetomotive force per unit length of motor, which, in turn, gives rise the air gap flux.

With the primary being three-phase supplied, a sinusoidally distributed magnetic flux will appear in the air gap. If a small element of material in the secondary sheet enters the zone of influence of the magnetic flux in the air gap, it will generate maximum eddy currents and reduce the flux to zero in that element of material, as to oppose the sudden variation. These eddy currents will then fade away and the magnetic flux will rise exponentially with time constant T_2. After this element goes through the whole air gap and reaches its exit, the opposite effect will occur: the magnetic flux will try to remain constant outside the air gap, as if it were a tail of magnetic flux, giving rise to eddy currents in the small element of secondary sheet material until the magnetic flux reaches zero. This decay will be much quicker than the rise during the entry with time constant T_2, related only to the leakage inductance of the secondary sheet. In order to plot this effect, the distance covered by the primary must be found, since the magnetic flux distribution in the air gap depends of the primary velocity (of the travelling wave). In terms of secondary time constants, the distance travelled by the primary is given by equation 3.2, with v_1 being the primary's velocity, that is to say, the velocity of the travelling wave created by the primary.

$$d_1 = v_1 T_2 \tag{3.2}$$

If the length of the primary is D, then the time taken for an element in the secondary

to travel D is

$$T_v = \frac{D}{v} \tag{3.3}$$

which can be expressed in terms of T_2

$$Q = \frac{T_v}{T_2} = \frac{DR_{2,1}}{(L_m + L_{2,1})v} \tag{3.4}$$

which can be seen as the normalised motor length Q, in regards to this time scale of the secondary. This equivalent motor length is related to the motor speed, and therefore enables a generic study of the linear induction motor for any velocity, exemplified in figure 3.3.

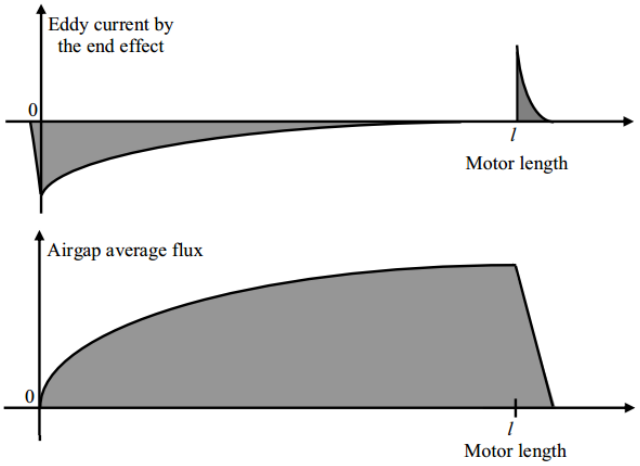

Figure 3.3: Entry build up and exit tail mechanisms described by Duncan [4].

The value of Q represents the motor's ability to resist the loss of output due to the end effects. The secondary eddy currents will act as demagnetising currents, opposing the magnetising current provided by the primary, as anti-phase currents or negative magnetomotive force per unit length. The demagnetising effect of the secondary current $I_{2,1avg}$ will be represented as an inductance in parallel with L_m, which carries a current $I_{2,1avg}$. The parallel of L_m and this new inductance results in equation 3.5. This branch carries the current $I_m = I_{m,1avg} + I_{2,1avg}$. If the velocity tends to zero, Q tends to infinity, and the new inductance will be equal to L_m.

$$L_m\Big(1 - \frac{1 - \exp(-Q)}{Q}\Big) \tag{3.5}$$

To take into account the losses produced by the eddy currents, the resistance R_{21} must be added to the magnetising branch, which will carry the current $I_{2,1}$. The total power due to the eddy current losses can then be given by equation 3.6.

$$P = I_{2,1RMS}^2 R_{2,1} = I_m R_{2,1} \frac{1 - \exp(-Q)}{Q} \tag{3.6}$$

Therefore, a resistor with $R_{2,1}\frac{1-\exp(-Q)}{Q}$ which will carry the current I_m can be conceptualized, which will reflect the power losses due to the end effects. Finally, the new equivalent circuit can be designed, as per figure 3.4.

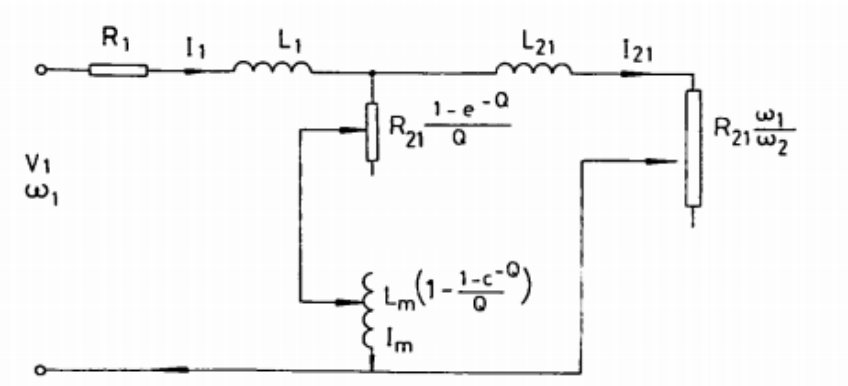

Figure 3.4: Linear induction motor's equivalent circuit proposed by Duncan [9].

This approach is very useful in order to do a simplified study of the influence on the motor's performance due to the end effects. However, nothing about the profile of the magnetic field itself in the air gap can be said.

3.1.3 d-q Axis and End Effect Constant

Using as basis the equivalent circuit obtained by Duncan [9], an analysis on the d-q axis is made [4], using the end effects. This analysis is useful in order to apply vector control to the linear induction motor. The q-axis of the equivalent circuit of the linear induction motor is the same as the q-axis for a rotary induction motor, and its parameters do

not vary due to the end effects. It is in the d-axis that appear the end effects in the linear induction motor. However, the magnetising branch in the d-axis equivalent circuit shows the new magnetising inductance which is affected by the eddy currents in the secondary, as well as the power losses on the secondary due to the eddy currents.

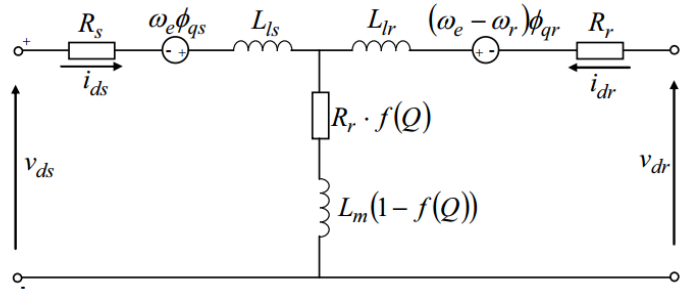

(a) d-axis equivalent circuit.

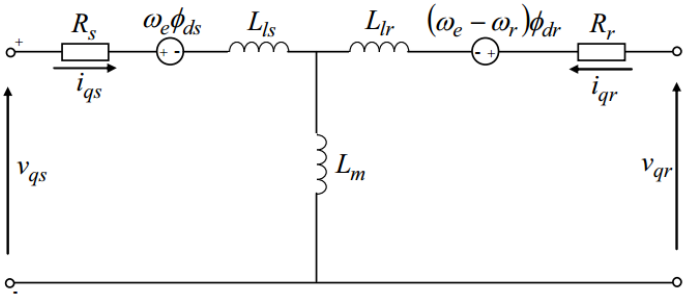

(b) q-axis equivalent circuit.

Figure 3.5: linear induction motor d-q axis equivalent circuits [4].

Taking into account the d-q axis circuits obtained in figure 3.5, it is now possible to calculate the motor's thrust, which will have in consideration the end effects. Thrust can then be expressed as a constant times current i_{qs}, as per equation 3.7, where P is the motor's mechanical power output, $f(Q)$ is given by Duncan's equivalent circuit, equal to $\frac{1-\exp(-Q)}{Q}$, and h is the pole-pitch.

$$F_e = K_f i_{qs} \tag{3.7a}$$

$$K_f = \frac{3}{2} P \frac{\pi L_m (1 - f(Q))}{h(L_r - L_m f(Q))} \phi_{dr} \tag{3.7b}$$

Chapter 4

One Dimensional Model

4.1 Theoretical Overview

In traditional cylindrical machines, the rotor is fully enveloped by the stator, meaning that every point on the surface of the rotor is subject at all times, in steady state, to a magnetic field provided by the stator. A shell-like stator introduces a discontinuity of the magnetic field from the standpoint of view of the rotor.

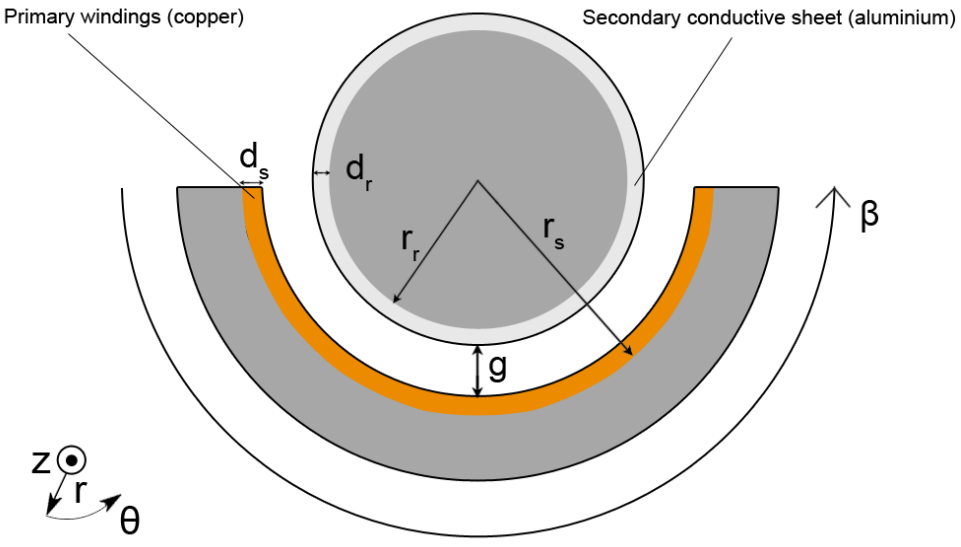

Figure 4.1: System coordinates.

A series of physical entities will be introduced. Firstly, it is considered that the radius

of the motor is r_s for the stator and r_r for the rotor. Equivalent conductive sheet's widths will be considered. That is to say, for the primary winding, a very thin conductive sheet will be considered instead. The same will be considered for the secondary sheet, and the real width will only be considered for the actual current densities, as will be discussed in section 4.1.4. Therefore, the equivalent air gap is given by $g = r_s - r_r + d_s + d_r$.

The primary current density is considered to be $\mathbf{j_1}$, while the secondary current density is $\mathbf{j_2}$. Finally, it is considered that the angle of the shell-like stator is β, that is to say, the primary envelopes the secondary in β radians.

4.1.1 Second order system

Following the methodology used in references [1], [5], a second order system can be obtained to describe the magnetic field in the air gap. In order to do so, an analysis through Ampère's law and electromotive force on the rotor is done.

Some approximations will be made. Firstly, the magnetic field is considered to be dependent of only the θ coordinate, meaning that $\mathbf{B}$ is constant along the r coordinate. In this sense, only a solution for $\mathbf{B_r}(t, \theta)$ is to be found. This can be a good approximation if the air gap is small enough.

4.1.2 Ampère's Law

Applying Ampère's law in the integral form in this cylindrical geometry results in equation 4.1.

$$\int_{r_r}^{r_s} \mathbf{H}(\theta = \theta_1)dr - \int_{r_r}^{r_s} \mathbf{H}(\theta = \theta_2)dr = \int_{\theta_1}^{\theta_2} \mathbf{j_1} r_s d\theta + \int_{\theta_1}^{\theta_2} \mathbf{j_2} r_r d\theta \tag{4.1}$$

Noting that, if between θ_1 and θ_2 the magnetic field varies in a linear way, that is to say, if $\Delta\theta = \theta_2 - \theta_1$ is very small, then the derivative of θ can be used to express left side of the equation.

$$\mathbf{H}(\theta = \theta_1) - \mathbf{H}(\theta = \theta_2) = -\Delta\theta \frac{\partial \mathbf{H}}{\partial \theta} \tag{4.2}$$

Finally, the solution of Ampère's law is given by equation 4.3,

$$-\frac{\partial \mathbf{B}}{\partial \theta} = \mu_0[\mathbf{j_1}(r_g + 1) + \mathbf{j_2} r_g] \tag{4.3}$$

where r_g is given by equation 4.4.

$$r_g = \frac{r_r}{g} \tag{4.4}$$

4.1.3 Electromotive Force

The Maxwell-Faraday equation in cylindrical coordinates is given by equation 4.5, with ω_r being the rotor speed.

$$\boldsymbol{\epsilon} = -\frac{\partial \mathbf{A}}{\partial t} - \omega_r \frac{\partial \mathbf{A}}{\partial \theta} \tag{4.5}$$

Making the substitutions referred in chapter 2, and differentiating the electromotive force expression in order of θ, results in equation 4.6.

$$\frac{\partial \boldsymbol{\epsilon}}{\partial \theta} = -r_r \frac{\partial \mathbf{B}}{\partial t} - \omega_r r_r \frac{\partial \mathbf{B}}{\partial \theta} \tag{4.6}$$

4.1.4 General Equation for the Magnetic Field

It is now possible to write an expression that represents the magnetic field in the air gap. Firstly, equivalent current densities will be considered, specifically in the secondary. That is to say that the width of the secondary conductor sheet will be considered, resulting in an equivalent secondary conductor resistivity, given by equation 4.7

$$\rho_s = \frac{\rho}{d_r} \tag{4.7}$$

where ρ is the rotor's resistivity and d_r is the thickness of the rotor's surface conducting material. Substituting the equation resulting from the electromotive force into the equation resulting from Ampère's law creates the general expression of the model, which can be seen in equation 4.8.

$$\frac{\partial^2 \mathbf{B}}{\partial \theta^2} - \mu_0 \frac{r_g r_r}{\rho_s} \frac{\partial \mathbf{B}}{\partial t} - \mu_0 \frac{r_g r_r \omega_r}{\rho_s} \frac{\partial \mathbf{B}}{\partial \theta} = -\mu_0 \frac{\partial \mathbf{j_1}}{\partial \theta} (r_g + 1) \tag{4.8}$$

4.2 Solution for the General Equation

The solution of the general equation will be done through typical analysis of differential equations. Firstly, a steady-sate solution will be found, which is expected to be a simple travelling wave. The transient solutions will be obtained through the homogeneous equation. Note that while it is called transient solution, as will be seen further ahead, these terms are persistent over time.

4.2.1 Steady-state Solution

In steady-state, it can be assumed that the magnetic field in the air gap is simply a travelling wave. This can be obtained if it is considered that no end-effects occur in the motor. In other words, in typical linear induction motor terms, it is considered that the motor length is infinite. Such notion makes no sense considering the cylindrical coordinates, and as such, a more appropriate analogy would be to consider that the motor length is $\beta = 2\pi$, or that the motor is a typical closed cylindrical rotary induction motor. This analysis is useful in order to calculate the magnetic field created by the primary windings alone, to which the end-effects will be added to.

It is assumed that the current density in the primary is given by equation 4.9, in which ω is the angular frequency of the power supply and k is the number of pair-poles.

$$\mathbf{j_1} = J_1 \exp\left[j(\omega t - k\theta)\right] \tag{4.9}$$

The amplitude J_1 is a real value representing an equivalent amplitude, in which the width of the primary conductive sheet is taking into account. Hence, $J_1 = \frac{J_M}{d_s}$, where J_M is the actual amplitude of the current density. Therefore, the magnetic field expression is given by 4.10.

$$\mathbf{B} = \overline{B_s} \exp\left[\jmath(\omega t - k\theta)\right] \tag{4.10}$$

Substituting the travelling wave in the general equation for the magnetic field given by equation 4.8, the amplitude of the travelling wave can be found in equation 4.11.

$$\overline{B_s} = -\frac{\jmath J_1 (r_g + 1) k \mu_0}{k^2 + \jmath \frac{r_g r_r \mu_0}{\rho_s} s\omega} \tag{4.11}$$

The slip of the motor s is defined in equation 4.12.

$$s = \frac{\omega - k\omega_r}{\omega} \tag{4.12}$$

It must be noted that the amplitude $\overline{B_S}$ is a complex number. This will also be true for any wave amplitude found ahead, which is why it is not necessary to consider a phase δ_s. This phase is implicit inside the amplitude of $\overline{B_S}$, if treated as a complex number. However, when dealing with computer software, it might be useful to consider only the real part of the total field, in which case the field may be expressed as shown in equation 4.13, where $\delta_s = angle\{\overline{B_s}\}$. From this point forward, this travelling wave shall be referred to as $\mathbf{B_s}$, which contains both the complex amplitude and the sinusoidal function of θ.

$$\mathbf{B} = |\overline{B_s}| \cos\left(\omega t - k\theta + \delta_s\right) = \mathbf{B_s} \tag{4.13}$$

4.2.2 Field Phasors

The expression of the magnetic field created by the secondary current can now be obtained [5]. Because the magnetic field created by the induced currents in the secondary opposes the magnetic field created by the primary, if the slip of the motor is $s = 0$, that is to say, there are no induced currents in the secondary, then the magnetic field in the air gap should be at its maximum. If $s = 1$, the magnetic field in the air gap should be at its minimum, as the induced currents in the secondary are at their maximum. Taking this into account, a new entity ϕ shall be introduced and a phasor

analysis will be made.

If it is considered that the amplitude given by 4.11 is a complex number, then its phase can be given by equation 4.14.

$$\tan\phi = \frac{r_g r_r \mu_0}{\rho_s k^2} s\omega \tag{4.14}$$

After assigning a new variable as per equation 4.15, then the amplitude of the travelling wave can be expressed as in equation 4.16.

$$B_M = \frac{J_1 \mu_0 (rg+1)}{k} \tag{4.15}$$

$$\mathbf{B_s} = -\jmath B_M \cos(\phi) \exp(-\jmath\phi) \tag{4.16}$$

Equation 4.16 is equivalent to equation 4.11. It is important to note that B_M is the amplitude of the travelling wave when the $s = 0$, meaning it is the maximum amplitude of the travelling wave in the air gap. As previously mentioned, the magnetic field created by the secondary currents will oppose the magnetic field created by the primary, in a way that, when $s = 0$ the field travelling wave has an amplitude B_M. Therefore, if $\mathbf{B_{si}}$ is the magnetic field created by the induced currents, then its form can be given by equation 4.17.

$$\mathbf{B_{si}} = \mathbf{B_s} - B_M \tag{4.17}$$

Looking at diagram 4.2, it is possible to see the relationship between the three fields. Finally, the expression of $\mathbf{B_{si}}$ can be obtained as per equation 4.18.

$$\mathbf{B_{si}} = \jmath B_M \sin(\phi) \exp(-\jmath\phi) \tag{4.18}$$

In terms of the travelling wave's amplitude, it can also be expressed as in equation 4.19.

$$\mathbf{B_{si}} = -\tan(\phi)\mathbf{B_s} \tag{4.19}$$

It must be noted that wave $\mathbf{B_s}$ has a phase in relation to $\mathbf{j_1}$, referred to as δ_s. In fact, if $s = 0$, then this phase δ_s is exactly $-\frac{\pi}{2}$.

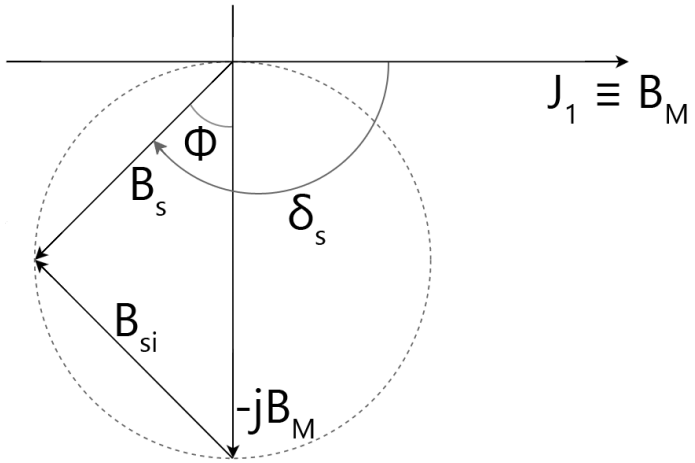

Figure 4.2: Phasors describing the relation between $\mathbf{B_s}$, $\mathbf{B_{si}}$ and B_M.

4.2.3 Transient Solution

The transient solution can be obtained through the homogeneous equation, meaning equalling the general equation to zero, as per equation 4.20.

$$\frac{\partial^2 \mathbf{B}}{\partial \theta^2} - \mu_0 \frac{r_g r_r}{\rho_s} \frac{\partial \mathbf{B}}{\partial t} - \mu_0 \frac{r_g r_r \omega_r}{\rho_s} \frac{\partial \mathbf{B}}{\partial \theta} = 0 \tag{4.20}$$

To solve the equation, it is needed to make some assumptions. Firstly, it will be assumed that the solution for the magnetic field is the multiplication of two terms: one time dependent and other θ dependent.

$$\mathbf{B}(t, \theta) = T(t)B(\theta) \tag{4.21}$$

Substituting in the general homogeneous equation, results in equation 4.22.

$$\frac{1}{T(t)}\frac{\partial T(t)}{\partial t} = \frac{1}{B(\theta)}\Big[\frac{\rho_s}{r_g r_r \mu_0}\frac{\partial^2 B(\theta)}{\partial \theta^2} - \omega_r \frac{\partial B(\theta)}{\partial \theta}\Big] \equiv \lambda \tag{4.22}$$

Looking at the left side of equation 4.22, the solution of $T(t)$ is easily obtained as per equation 4.23, resulting in equation 4.24.

$$\frac{1}{T(t)}\frac{\partial T(t)}{\partial t} = \lambda \tag{4.23}$$

$$T(t) = C\exp(\lambda t) \tag{4.24}$$

It must be noted that, due to the nature of the power supply given in equation 4.9, λ can only be equal to equation 4.25.

$$\lambda = \jmath\omega \tag{4.25}$$

Another method is to solve the general equation with the help of complex numbers. In that way, the derivative in order of time $\frac{\partial}{\partial t} = j\omega$, which simplifies the problem. If this analysis is taken, it becomes obvious that the statement in equation 4.25 is correct.

Looking at the right side of equation 4.20, taking into account that $B(\theta) = |\overline{B}|\exp(\jmath k\theta)$ as shown in equation 4.10, results in the characteristic equation 4.26, after using the Laplace Transformation, where $TL\{\frac{\partial}{\partial\theta}\} = s$.

$$s^2 - \frac{\omega_r r_g r_r \mu_0}{\rho_s}s - \frac{\jmath\omega r_g r_r \mu_0}{\rho_s} = 0 \tag{4.26}$$

Solving the 2nd order equation with B as the variable, gives two solutions as per equation 4.27.

$$\overline{s_1}, \overline{s_2} = \frac{1}{2}\frac{\omega_r r_g r_r \mu_0}{\rho_s} \mp \frac{1}{2}\sqrt{\Big(\frac{\omega_r r_g r_r \mu_0}{\rho_s}\Big)^2 + \jmath\frac{4\omega r_g r_r \mu_0}{\rho_s}} \tag{4.27}$$

In order to find the solutions $\overline{s_1}, \overline{s_2}$ it will be first considered the squared root only, separating the real and imaginary values, as shown in equation 4.28, where $X > 0$ and

$Y > 0$.

$$\sqrt{\left(\frac{\omega_r r_g r_r \mu_0}{\rho_s}\right)^2 + \jmath\frac{4\omega r_g r_r \mu_0}{\rho_s}} = X + \jmath Y \tag{4.28}$$

Now, solutions s_1, s_2 can be expressed as per equations 4.29 and 4.30.

$$\overline{s_1} = \frac{\omega_r r_g r_r \mu_0 - \rho_s X}{2\rho_s} - \jmath\frac{Y}{2} \equiv -\frac{1}{\alpha_1} - \jmath k_e \tag{4.29}$$

$$\overline{s_2} = \frac{\omega_r r_g r_r \mu_0 + \rho_s X}{2\rho_s} + \jmath\frac{Y}{2} \equiv \frac{1}{\alpha_2} + \jmath k_e \tag{4.30}$$

$$\alpha_1 = \frac{2\rho_s}{\rho_s X - \omega_r r_g r_r \mu_0} \tag{4.31}$$

$$\alpha_2 = \frac{2\rho_s}{\rho_s X + \omega_r r_g r_r \mu_0} \tag{4.32}$$

$$k_e = \frac{Y}{2} \tag{4.33}$$

This will result in a sum of two waves for the transient solution, in the form of expression 4.34.

$$\overline{B_1}\exp\left(\overline{s_1}\theta\right)\exp\left(\jmath\omega t\right) + \overline{B_2}\exp\left(\overline{s_2}\theta\right)\exp\left(\jmath\omega t\right) = \mathbf{B_1} + \mathbf{B_2} \tag{4.34}$$

The transient solution shows two waves, $\mathbf{B_1}$ and $\mathbf{B_2}$. The first wave will be called the entry end effect wave, while the second wave will be called the exit end effect wave. The reason for this will become clear when the boundary conditions are defined. The first wave $\mathbf{B_1}$ is related to the discontinuity of the iron core in the vicinity of the entry of the air gap, in relation to the rotating direction in θ of the motor. Similarly, the wave $\mathbf{B_2}$ is related to the same discontinuity near the exit of the air gap.

The terms α_1 and α_2 will be referred to as the penetration angles, in rad. They are related to the length of air gap, in the θ coordinate, which is reached by each wave, meaning that the wave $\mathbf{B_1}$ will reach a greater length of the air gap, in the θ coordinate, if α_1 is greater. The same is applicable to the $\mathbf{B_2}$ wave and α_2, however in different directions. Note that the wave $\mathbf{B_1}$ travels in the negative direction of θ, while $\mathbf{B_2}$ travels

in the positive direction of θ.

The term k_e is related to the speed of these end effect waves in the θ coordinate, which can be different from the speed of the travelling wave $\mathbf{B_s}$, related to the electric speed as per $\frac{2\pi f}{k}$. Therefore, the speed of the end effect waves is given by equation 4.35.

$$\omega_e = \frac{2\pi f}{k_e} \tag{4.35}$$

Further ahead in this work, a relation between speeds ω_e and the synchronous speed ω_s will be determined, which will vary according to the type of motor considered: high speed or low speed motors.

4.2.4 General Solution

The general solution for the equation 4.8 will be the sum of the steady-state solution and the transient solution, resulting in equation 4.36.

$$\begin{aligned}\mathbf{B}(t,\theta) =& \overline{B_s}\exp\left[\jmath(\omega t - k\theta)\right] \\ &+\overline{B_1}\exp\left(-\frac{\theta}{\alpha_1}\right)\exp\left[\jmath(\omega t - k_e\theta)\right] \\ &+\overline{B_2'}\exp\left(\frac{\theta}{\alpha_2}\right)\exp\left[\jmath(\omega t + k_e\theta)\right]\end{aligned} \tag{4.36}$$

This solution represents the magnetic field in the air gap, which is both a function of time and space. The first wave is the travelling wave, which travels in the negative direction of θ. The second wave also travels in the negative direction of θ and is damped by $-\frac{1}{\alpha_1}$. The last wave travels in the positive direction of θ and is damped by $\frac{1}{\alpha_2}$.

Since the wave $\mathbf{B_2}$ is supposed to exist only nearby the exit of the motor, it is advantageous for computer simulations that a new reference for θ is considered for this wave, as using expression 4.36 would result in overflow due to the positive exponential [5]. Therefore, it is more advantageous to consider the solution as expressed by 4.37. Note

that a different complex amplitude $\overline{B_2}$ from $\overline{B_2'}$ is to be found.

$$\begin{aligned}\mathbf{B}(t,\theta) =& \overline{B_s}\exp\left[\jmath(\omega t - k\theta)\right] \\ &+\overline{B_1}\exp\left(-\frac{\theta}{\alpha_1}\right)\exp\left[\jmath(\omega t - k_e\theta)\right] \\ &+\overline{B_2}\exp\left(\frac{\theta-\beta}{\alpha_2}\right)\exp\left[\jmath(\omega t + k_e(\theta-\beta))\right] \\ =& \mathbf{B_s} + \mathbf{B_1} + \mathbf{B_2}\end{aligned} \tag{4.37}$$

4.2.5 Boundary Conditions

In order to find the amplitudes of the end-effect waves $\mathbf{B_1}$ and $\mathbf{B_2}$, the boundary conditions must be found. Many different approaches are considered by [1], [5], such as an infinitely long motor and consideration of the return path losses in the rotor surface. Here, the most basic approach will be explored, but some notes about the other methods will be made.

The basic approach will be to consider that the full length of the air gap in the θ coordinate is under the influence of the primary current density $\mathbf{j_1}$. Due to this, a good approximation would be to also consider that, outside the air gap, the secondary current density $\mathbf{j_2}$ is zero, which means no induced currents exist outside of the air gap. Finally, if a small domain on the surface of the rotor not under the air gap is considered, it should not be under the influence of any current or magnetic field. As this domain enters the zone under the air gap, it will be subject to a big variation of the magnetic flux, as explained in the opening chapters. Therefore, another good approximation would be to consider that, near the entry and exit ends of the motor, $\frac{\partial}{\partial\theta} \gg \frac{\partial}{\partial t}$.

With these simplifications, it is possible to come up with a set of simple equations that enable the discovery of amplitudes $\mathbf{B_1}$ and $\mathbf{B_2}$. Firstly, the secondary current density, near the entry and exit ends, can now be expressed as per equation 4.38.

$$\mathbf{j_2} = -\frac{\omega_r r_r}{\rho_s}\mathbf{B} \tag{4.38}$$

Another boundary condition can be given by the flux conservation. If it is considered that magnetic fields exist only inside the air gap, then equation 4.39 can be used.

$$\int_0^{\beta} (\mathbf{B_s} + \mathbf{B_1} + \mathbf{B_2}) d\theta = 0 \tag{4.39}$$

This equation, when solved for $\mathbf{B_2}$, results in expression 4.40.

$$\overline{B_2} = \frac{-\overline{s_2}\left(\frac{\overline{B_s}[\jmath - \exp(-\jmath k\beta)]}{k} - \frac{\overline{B_1}[\exp(\overline{s_1}\beta) - 1]}{\overline{s_1}}\right)}{\exp(-\overline{s_2}\beta) - 1} \tag{4.40}$$

Using now the new current density expression near the entry, or $\theta = 0$, remembering that the total magnetic field inside the air gap is given by 4.37, and that, from 4.3, equation 4.41 is true, then the equation 4.42 is also true.

$$\mathbf{j_2} = -\frac{1}{\mu_0 r_g}\frac{\partial \mathbf{B}}{\partial \theta} - \mathbf{j_1}\left(1 + \frac{1}{r_g}\right) \tag{4.41}$$

$$\mathbf{B}|_{\theta=0} = -\frac{1}{\mu_0 r_g}\frac{\partial \mathbf{B}}{\partial \theta}|_{\theta=0} - \mathbf{j_1}|_{\theta=0}\left(1 + \frac{1}{r_g}\right) \tag{4.42}$$

From this equation, the amplitude of wave $\mathbf{B_1}$, or rather, $\overline{B_1}$, can be obtained. The expression can be found in appendix A, under equation A.1.

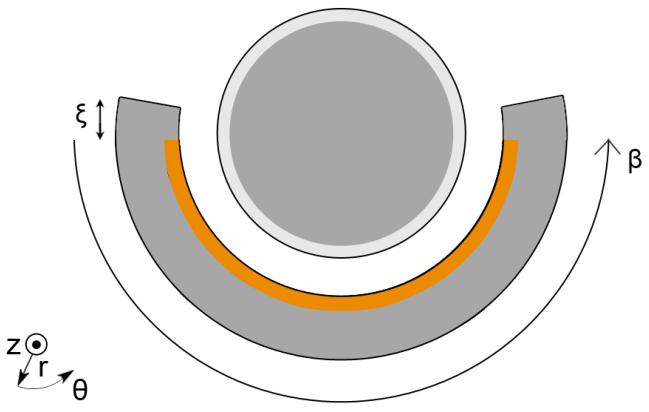

Figure 4.3: Second set of boundary conditions, considering a ξ angle with no primary winding.

Another set of boundary conditions can be found if it is considered that fringing occurs at the edges of the motor. Fringing can be described as the existence of magnetic field outside of the air gap, in the vicinity of the entry and exit ends of the motor. This is in accordance to the model explained by [9] and summarized in the first chapters of this work, and goes against the first considerations taken for the boundary conditions of the method above. The simplest approach for these new set of boundary conditions is to consider a small angle ξ in which the magnetic field exists outside the air gap, as per figure 4.3, and apply the magnetic flux conservation as per equation 4.43.

$$\int_{-\xi}^{\beta+\xi} (\mathbf{B_s} + \mathbf{B_1} + \mathbf{B_2}) d\theta = 0 \tag{4.43}$$

The expression for $\mathbf{B_1}$ will remain the same, but amplitude $\mathbf{B_2}$ will adjust itself to the larger zone that the magnetic field can exist, and as such will suffer alterations.

These boundary conditions depend on the value of ξ, and its value cannot be easily obtained. As such, a number of tests will be performed in section 6.2 and compared with a Finite Element Analysis software, using the first set of simpler boundary conditions. Afterwards, taking into account the differences in results between the model and Finite Element Analysis software, a value for ξ will be estimated and the second set of boundary conditions will be applied.

Chapter 5

Model Analysis

The aim of this chapter is to analyse how the different parameters of the model obtained before vary with the parameters of the motor, as well as make some statements about the implications of the parameters and their meaning.

5.1 Penetration Depths and End Effect Wave Speed

The terms α_1 and α_2 are fundamental to the model previously obtained, as they can provide a direct measure of the influence of the end effects in the magnetic field inside the air gap. The term k_e also has some interesting influences in the motor's performance, implying different speeds for different waves. Therefore, the study of these parameters' sensitivity is paramount to understand the motors' performance with different configurations.

For the examples provided next, the general motor parameters are given by table 5.1, unless otherwise specified. These parameters are based off the prototype available in our laboratory, as designed by this work's supervisor [10].

5.1.1 Air Gap Variation

The variation of the air gap g will influence the penetration depths α_1 and α_2 in a way which is not obvious, looking just at expressions 4.31 and 4.32, as it presents a compli-

Frequency f	50 Hz
Number of pole-pairs k	2
Primary sheet width d_s	1 mm
Secondary sheet width d_r	1 mm
Rotor radius r_r	135 mm
Air gap length g	3 mm
Stator angle β	π rad
Secondary sheet resistivity ρ_s	2.6497x10^{-5} Ω
Primary current density J_M	5.5x10^6 A/m

Table 5.1: Motor parameters used for model's parameters' plots.

cated relationship with g. Therefore, it is not easy to interpret the effects of the variation of g in the overall end effects and motor performance. This relationship is plotted for various air gaps, ranging from 15 mm to 35 mm, as seen in figures 5.1, 5.2 and 5.3, and its results are discussed in section 5.1.6.

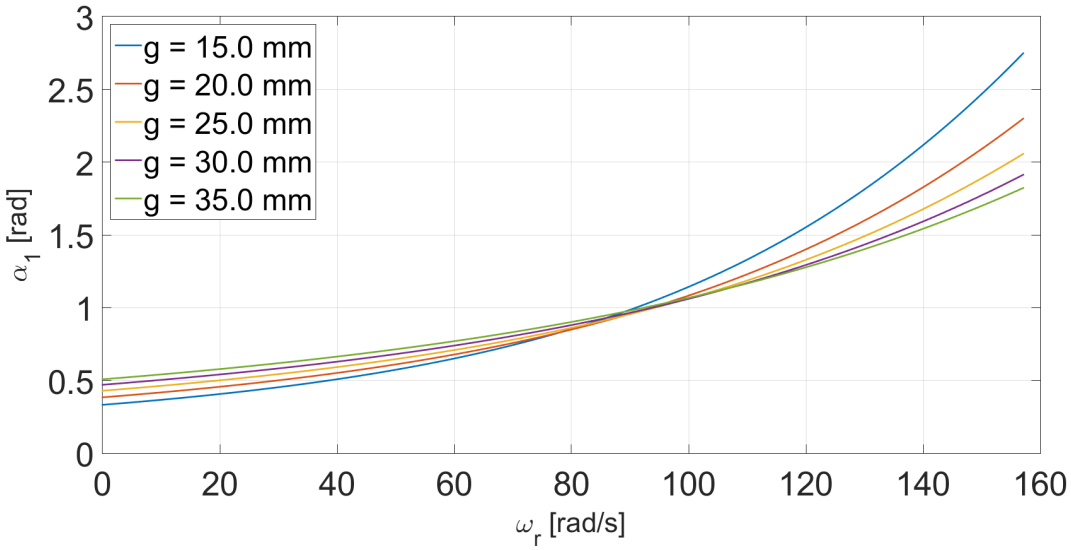

Figure 5.1: α_1 for various air gaps.

Looking at the previous figures, it becomes clear that, except for very low speed, α_1 is greater than α_2. Remembering the transient solutions of the field in equation 4.37, it can be considered that, if α_2 is small, then near the entrance, $\exp\left(-\frac{\beta}{\alpha_2}\right) \sim 0$, and as such $\mathbf{B_2}$ can be disregarded near the entrance, and in fact in most of the length of the

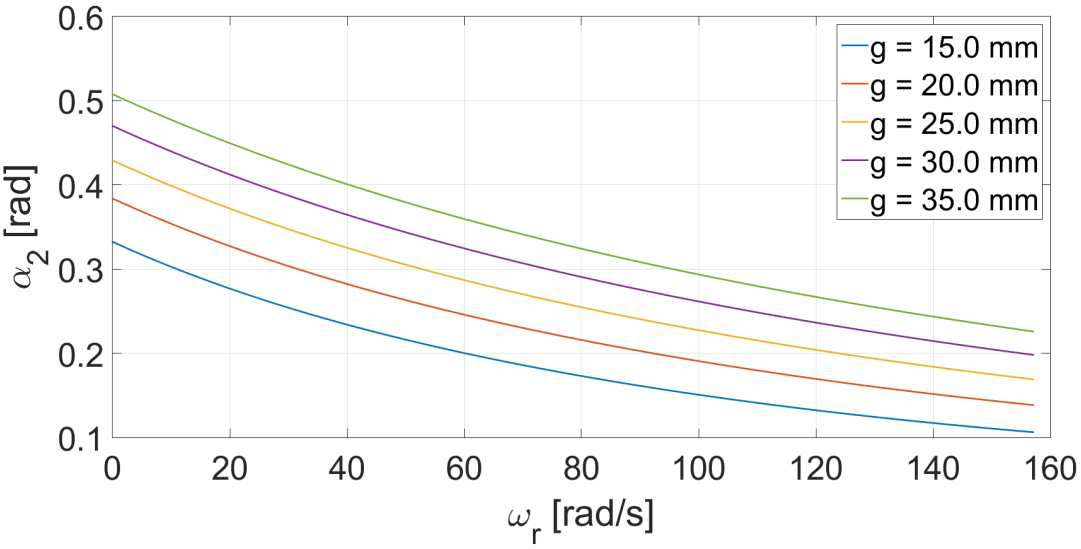

Figure 5.2: α_2 for various air gaps.

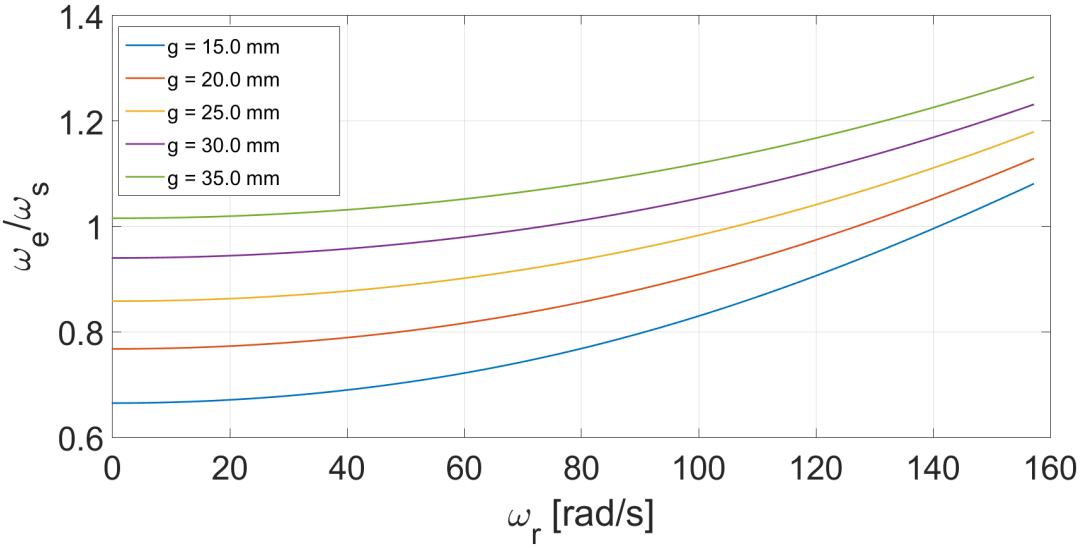

Figure 5.3: ω_e for various air gaps.

air gap, except near the exit. This means that the magnetic field in the majority of the air gap is influenced by just $\mathbf{B_s}$ and $\mathbf{B_1}$, as for the wave $\mathbf{B_1}$, near the entry, $\exp\left(-\frac{0}{\alpha_1}\right) = 1$. Therefore, it now becomes clear that the $\mathbf{B_1}$ wave is much more important to the performance of the motor than the $\mathbf{B_2}$ wave, as it influences the magnetic field in a much larger length than the latter.

5.1.2 Secondary Resistivity Variation

Similarly to the variation of g, α_1 and α_2 also have a complex relationship with the secondary sheet's resistivity ρ_s. The plots representing this relationship are presented in figures 5.4, 5.5 and 5.6.

The terms α_1 and α_2 seem to share the same behaviour as with the variation of g. However, k_e for the ρ_s variation has an interesting behaviour, in which the speed ω_e tends to ω_r for lower slips, which means that in fact ω_r becomes closer to ω_s. Therefore, k_e becomes approximately k for high speeds.

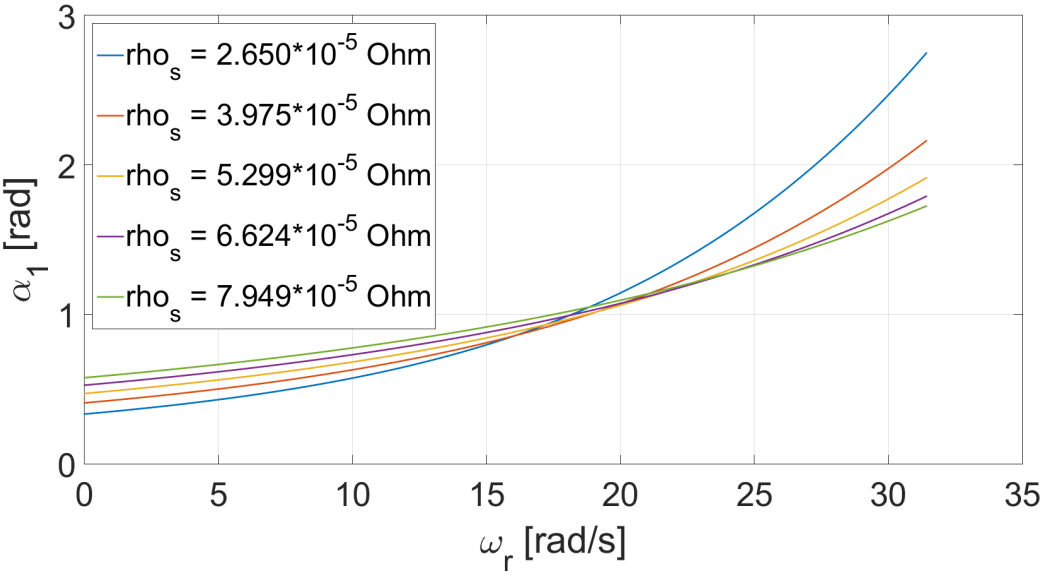

Figure 5.4: α_1 for various secondary resistivities.

5.1.3 Rotor Radius Variation

Rotor radius is one of the most important parameters in the spherical rotor motor, as it will be the main motor parameter to be considered when thinking about different applications of the motor. Again, its influence in the end effects is unclear, and the corresponding plots can be found in figures 5.7, 5.8 and 5.9.

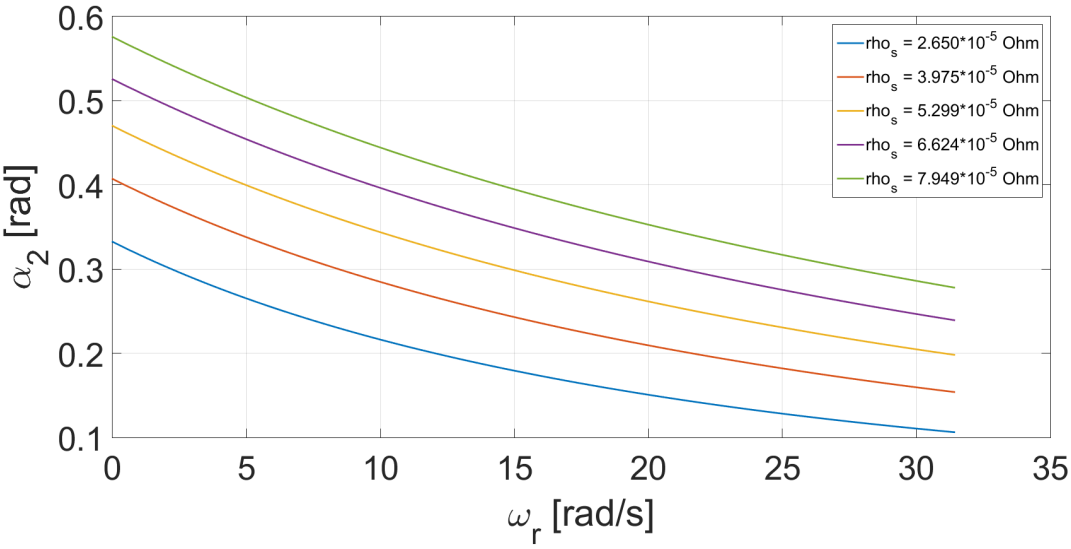

Figure 5.5: α_2 for various secondary resistivities.

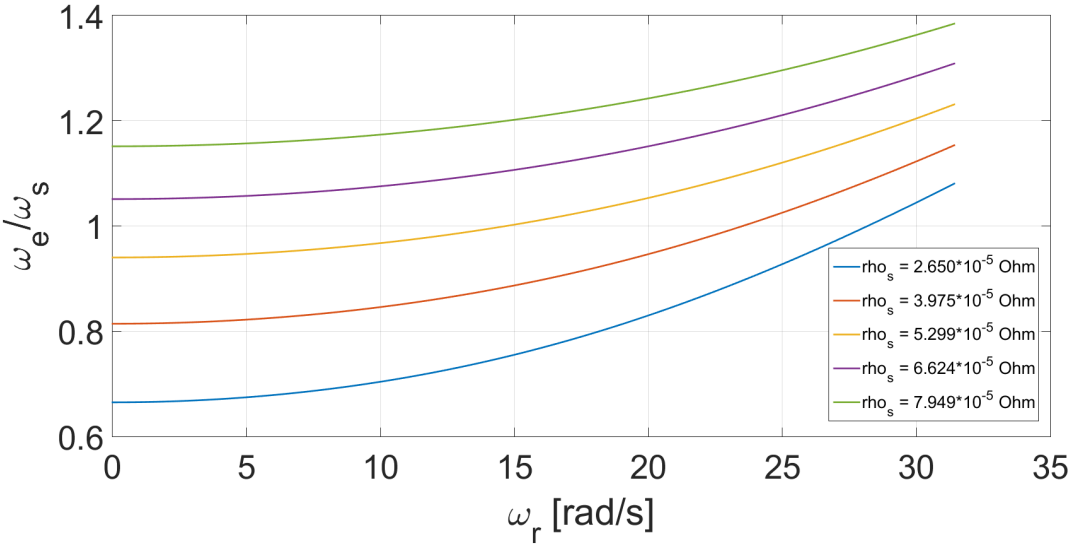

Figure 5.6: ω_e for various secondary resistivities.

5.1.4 Power Supply's Frequency Variation

The power supply's frequency might be another interesting parameter in which to assess the end effects with, as most induction motors are connected to the grid via an electronic speed controller, such as V/f. Variation of the model's parameters for various frequencies are given in plots 5.10, 5.11 and 5.12.

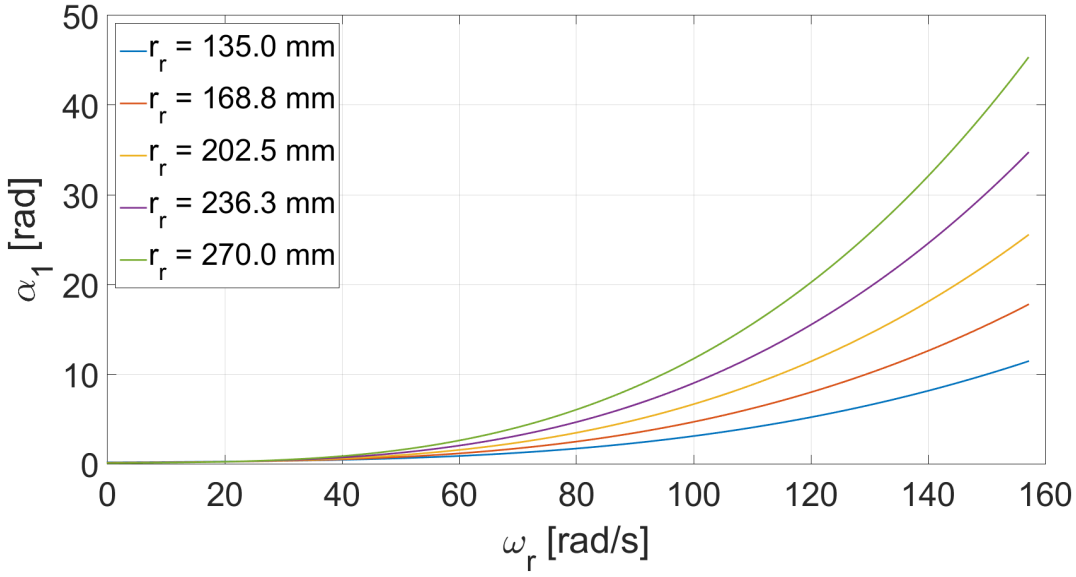

Figure 5.7: α_1 for various rotor radiuses.

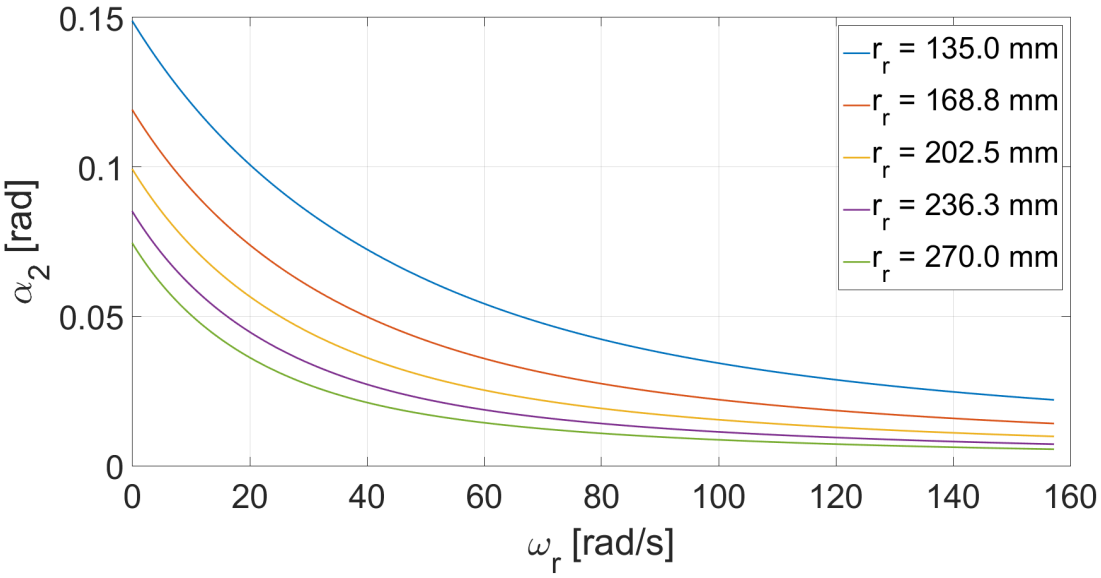

Figure 5.8: α_2 for various rotor radiuses.

5.1.5 Stator Angle

The β parameter represents the stator length in the θ coordinate. It would be expected that, if $\beta = 2\pi$, a typical cylindrical rotary motor would be obtained, when considering the cylindrical coordinates. However, in the proposed model, particularly during the

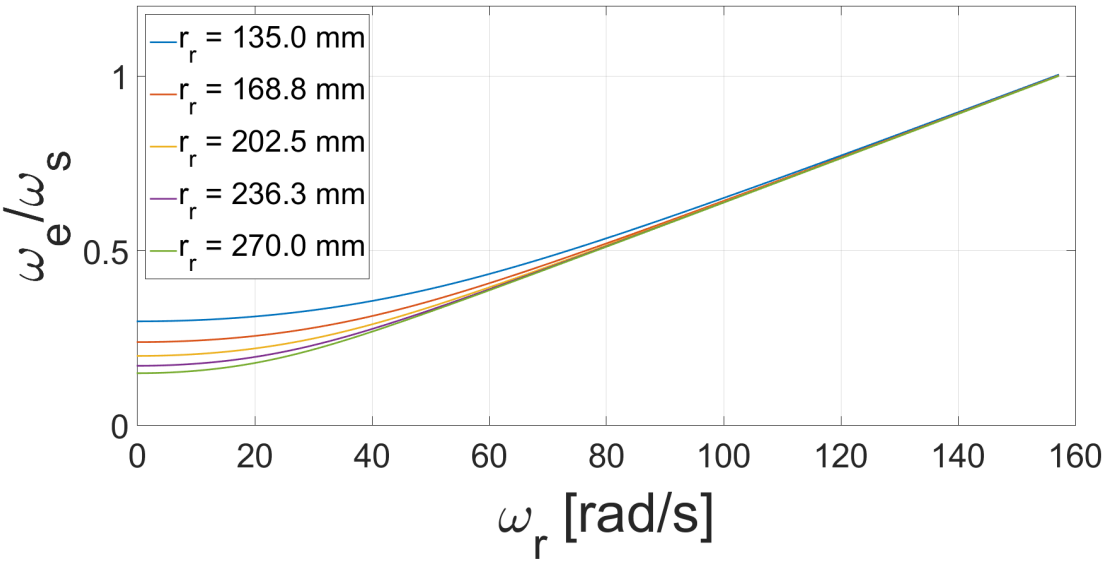

Figure 5.9: ω_e for various rotor radiuses.

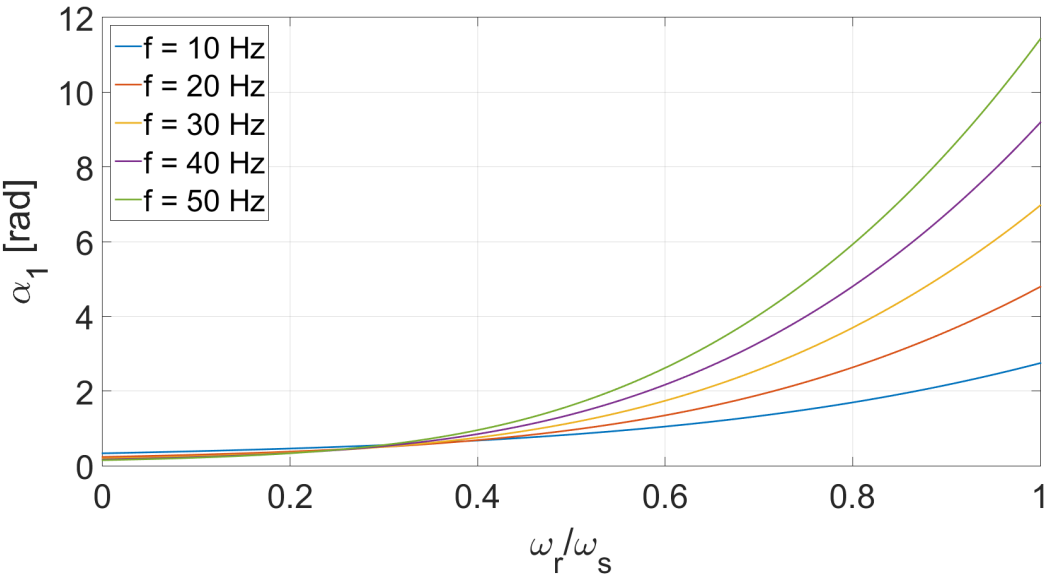

Figure 5.10: α_1 for various frequencies.

analysis of the boundary conditions, no special condition was considered for this case. Hence, the β does not truly represent the stator length in the θ coordinate for angles near 2π, as this model is not prepared to handle such case. The current model will consider β as if it were a length in the linear induction motor, and not an actual angle limited to 2π. However, it should be possible to consider better defined boundary con-

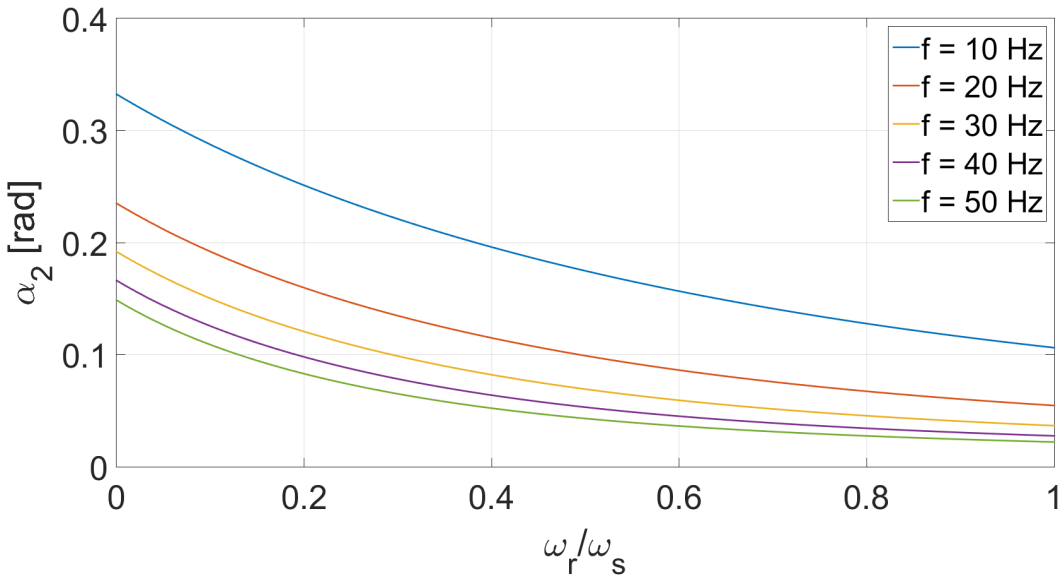

Figure 5.11: α_2 for various frequencies.

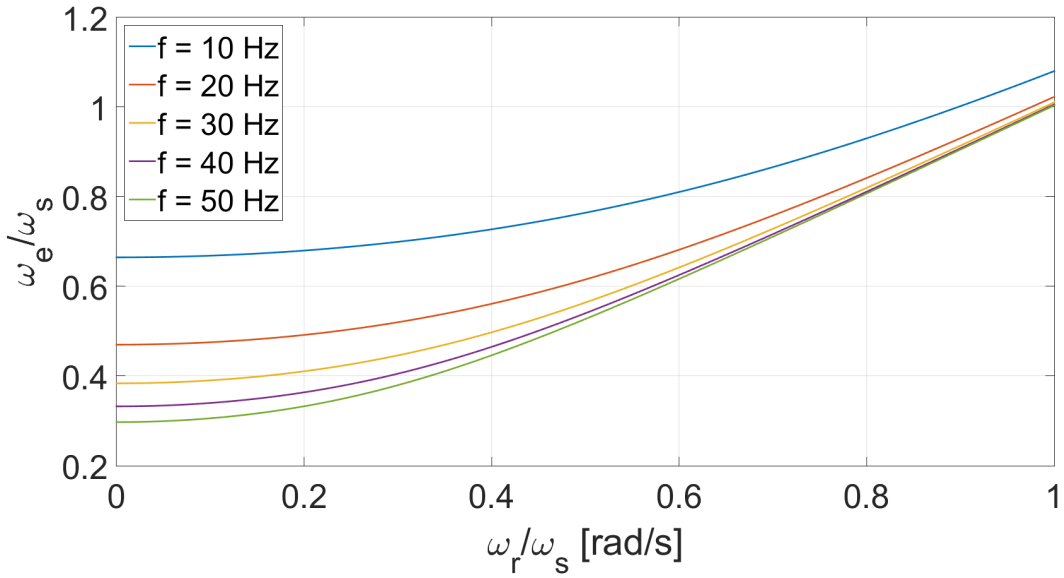

Figure 5.12: ω_e for various frequencies.

ditions in order to take this particular case in account, in such a way that, if $\beta = 2\pi$, then no end effects should occur, and a single travelling wave created by the primary current density should appear inside the air gap.

5.1.6 High Speed and Low Speed Motors

Up until this point, little considerations have been made about the motor itself, except perhaps the consideration of a small air gap. However, it is now impossible not to categorize motors, particularly by their speed. As shown in the variations of α_1, in figures 5.1, 5.4, 5.7 and 5.10 there seems to be an inversion of behaviour of the model's parameters between high speed and low speed. For example, α_1 for high speeds is larger for smaller air gaps, but for low speeds, α_1 is larger for larger air gaps. This behaviour is persistent in the variation of all the parameters presented before.

Looking at equation 4.28, it should be possible to make a separation between low and high speed motors. Taking the first term and dividing by the second term, we end up with constant γ in equation 5.1.

$$\gamma = \frac{r_g r_r \mu_0 \omega_r^2}{4\omega\rho_s} \tag{5.1}$$

Because the term ω_r is squared, a separation between speeds can be made. Therefore, if ω_r is very big, then $\gamma \gg 1$. If ω_r is small, then $\gamma < 1$. For high speed motors, this implies simplifications of the model. For example, equation 4.28 now becomes equation 5.2.

$$\frac{r_g r_g \mu_0 \omega_r}{\rho_s} + j\frac{2\omega}{\omega_r} \equiv X + jY \tag{5.2}$$

Therefore, the constant k_e which relates to the speed of the end effect waves, can now be expressed as per equation 5.3, and hence ω_e can be expressed as in 5.4.

$$k_e = \frac{Y}{2} = \frac{k}{1-s} \tag{5.3}$$

$$\omega_e = \frac{2\pi f}{k_e} = \frac{2\pi f(1-s)}{k} = \omega_r \tag{5.4}$$

Now, it is clear that once the speed of the motor becomes high enough, the speed of the end effect waves becomes the same as the motor speed. This can be observed

running the previous tests for a high speed motor, as seen in figure 5.9. The parameter γ results in $\gamma = 4.52$ for the last $r_r = 270mm$ and $\omega_r = 31.4rad/s$, which means that the motor can be considered to be a high speed motor, under those specifications.

For low speed motors, speed ω_e can be different from the motor speed ω_r, which will have implications on the output thrust, examined in 5.3.1.

5.2 Waves' Amplitudes

The amplitudes of each wave, $\mathbf{B_S}$, $\mathbf{B_1}$ and $\mathbf{B_2}$, for varying slip, are important in order to understand their interaction when considered together, which will be done in the chapter 6. The motor parameters used follow the ones in table 5.1, with frequency $f = 10Hz$.

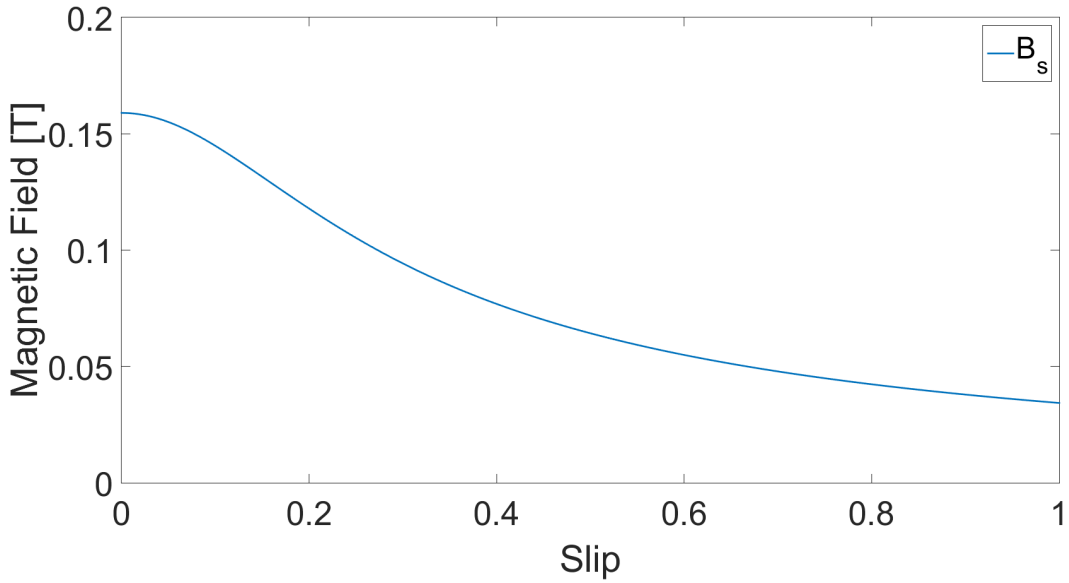

Figure 5.13: Amplitude of wave $\mathbf{B_S}$ for varying slips.

As expected, for lower motor speeds, the influence of the end effect waves drops significantly. For wave $\mathbf{B_1}$, it is interesting to note that its amplitude for low slips is similar to that of wave $\mathbf{B_S}$. However, this is not true for higher slips, having considerably more impact than wave $\mathbf{B_S}$. For low slips, wave $\mathbf{B_2}$ has a very high amplitude. However, as explained, due to the fact that wave's $\mathbf{B_2}$ penetration angle α_2 is very small, its

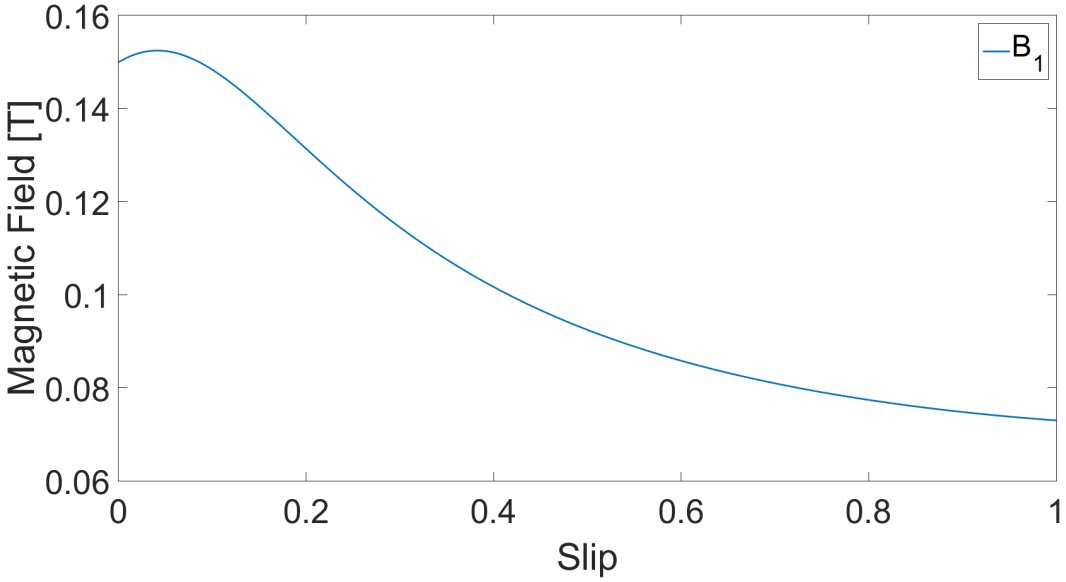

Figure 5.14: Amplitude of wave $\mathbf{B_1}$ for varying slips.

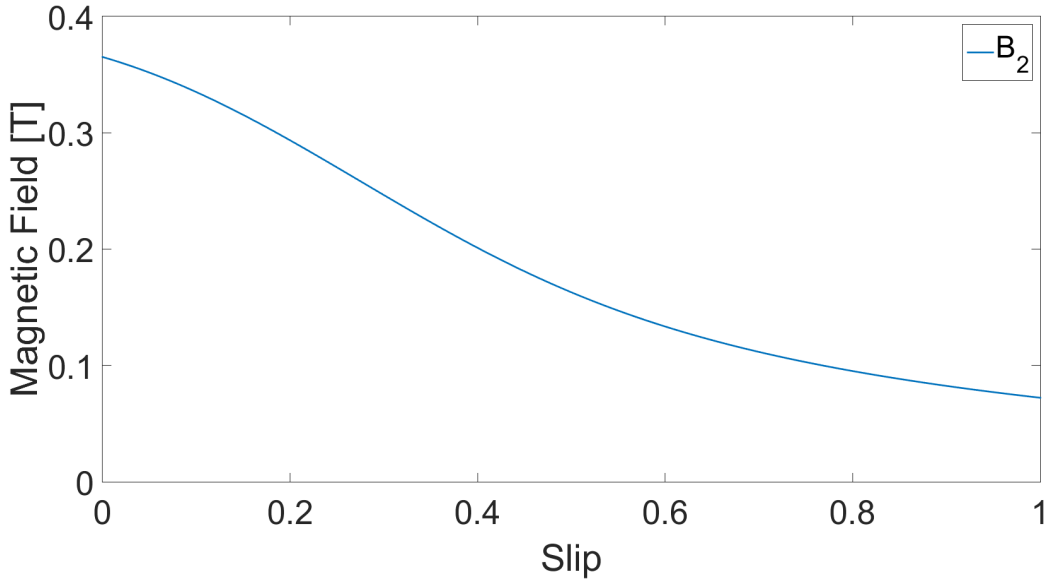

Figure 5.15: Amplitude of wave $\mathbf{B_2}$ for varying slips.

influence in the air gap spans a very limited arc length. For high slips, it has similar amplitude to that of wave $\mathbf{B_1}$.

5.3 Thrust

Thrust curves were computed for all slips. Again, separation between high and low speed motors has been made. For the low speed curve, a grid frequency of 10 Hz was chosen, while for the high speed curve, 150 Hz was chosen.

Two curves are plotted: the first curve is considering only the magnetic field $\mathbf{B_S}$ due to the primary windings, while the second curve is considering both $\mathbf{B_S}$ and $\mathbf{B_1}$. The first curve may be considered as the thrust curve obtained if no end effects were in action, equivalent to the typical rotary induction motor's thrust curve. The second curve includes the influence of the end effect wave $\mathbf{B_1}$ but not $\mathbf{B_2}$, in order to more easily obtain an analytical expression for the thrusts. This simplification is reasonable, as it has been proven that wave $\mathbf{B_2}$ exists mainly in the near exit end of the motor, and its influence on motor performance is reduced [1], [5].

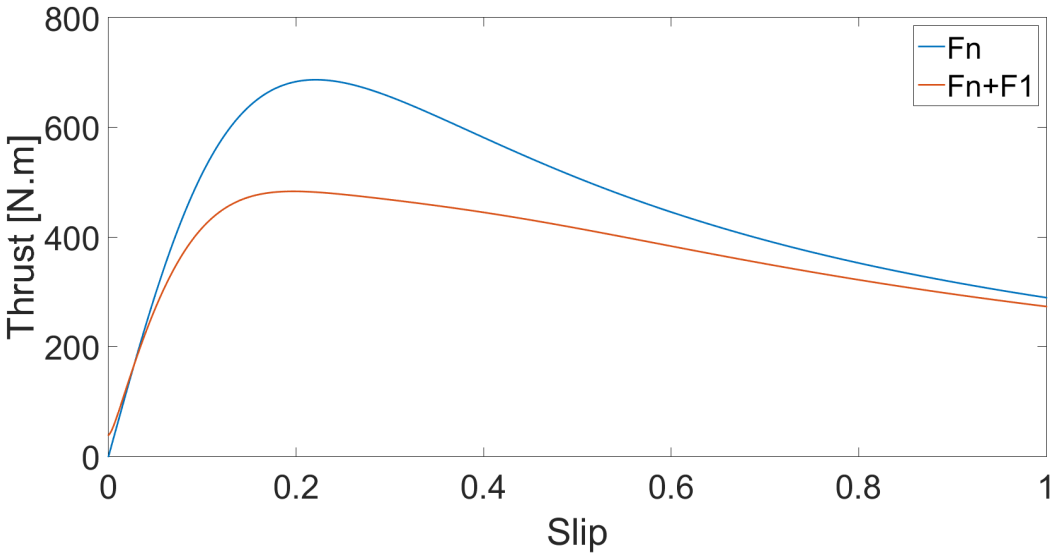

Figure 5.16: Thrust curves for a low speed motor.

The main result is that, when taken into account wave $\mathbf{B_1}$, the maximum output thrust is reduced. However, interesting behaviours for high and low slips occur in high and low speed motors, respectively. These phenomenons will be explored and analysed in section 5.3.1.

The thrust analytical expressions obtained derive from equation 5.5 [5], [10].

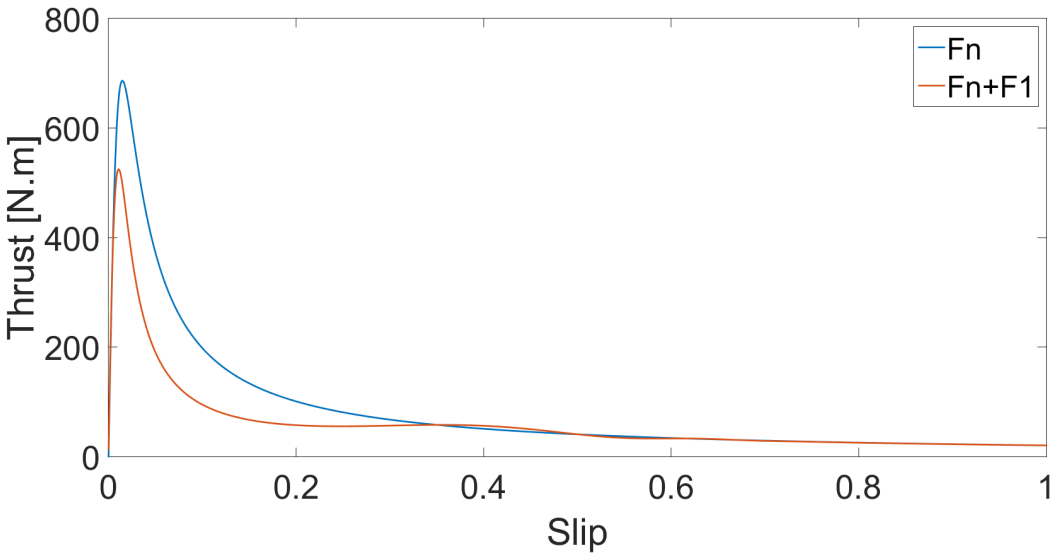

Figure 5.17: Thrust curves for a high speed motor.

$$\mathbf{F} = \mathbf{j_1} \times \mathbf{B} \tag{5.5}$$

Averaging over a period and integrating over the motor length, the thrust F_n due to the primary windings alone, becomes equation 5.6.

$$F_n = -\frac{1}{2}\int_0^{\beta} Re\{\mathbf{j_1}\mathbf{B_s}\}d\theta = \frac{J_1|\overline{B_S}|}{2}\left(\beta\cos(\delta_s) - \frac{1}{2k}(\sin(-2k\beta + \delta_s) - \sin(\delta_s))\right) \tag{5.6}$$

To take into account thrust due to wave $\mathbf{B_1}$, equation 5.5 must consider the field $\mathbf{B_1}$. The resulting thrust F_1's expression can be found in appendix B, under equation B.1 [1].

5.3.1 Phasor Analysis

For high speed motor's thrust, in figure 5.17, the most interesting phenomenon occurring is the oscillation of the thrust with larger slips. For low speed motors, figure 5.16, non null thrust at slip $s = 0$ is observed. To explain these phenomenons, it is necessary to analyse the relative motion of the magnetic field waves inside the air gap.

Firstly, it must be noted that in these diagrams, phasors $\mathbf{B_s}$ and $\mathbf{j_1}$ are stationary,

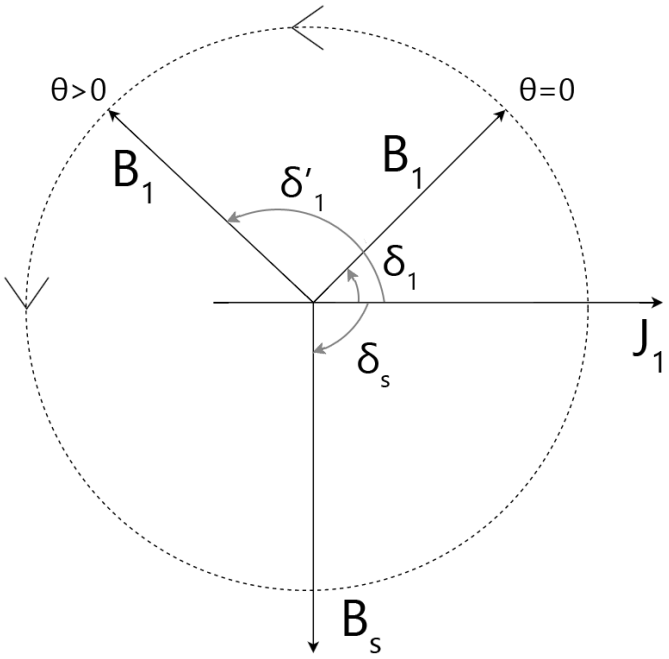

Figure 5.18: $\mathbf{B_1}$ phasors representation for a low speed motor, at $s = 0$.

that is to say, the reference is solidary with the travelling speed of phasors $\mathbf{B_s}$ and $\mathbf{j_1}$, which is the synchronous speed ω_s. Waves $\mathbf{B_1}$ and $\mathbf{B_2}$ travel at speed ω_e, which can be different from ω_s as observed in the previous figures 5.3, 5.6, 5.9 and 5.12. Therefore, waves $\mathbf{B_1}$ and $\mathbf{B_2}$ are phasors whose phases are varying in time, due to having a relative speed $\omega_e - \omega_s$ in respect to $\mathbf{B_s}$ and $\mathbf{j_1}$.

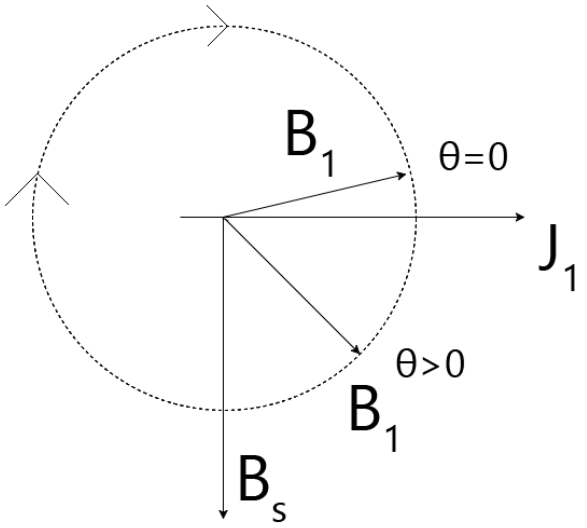

Figure 5.19: $\mathbf{B_1}$ phasors representation for a high speed motor, at $s \neq 0$.

For high speed motors, as seen in section 5.1.6, it can be considered that $\omega_e = \omega_r$. Therefore, if ω_r is lower than ω_s, then ω_e is also lower than ω_s. In this case, it's as if waves $\mathbf{B_1}$ and $\mathbf{B_2}$ are moving in relation to $\mathbf{B_s}$ and $\mathbf{j_1}$. For this analysis, only wave $\mathbf{B_1}$ will be considered, as its influence spans a greater length of air gap than wave $\mathbf{B_2}$, whose importance can be in most cases neglected. Wave $\mathbf{B_1}$ has a constant phase in relation to $\mathbf{B_s}$, due to its complex amplitude $\overline{B_1}$, which will be called δ_1. As this wave travels along the θ coordinate, because its speed is greater than the $\mathbf{B_s}$ wave, the relative phase to $\mathbf{B_s}$ will become smaller. Therefore, wave $\mathbf{B_1}$ can be represented as a phasor moving in the clockwise direction, with greater θ, as per figure 5.19.

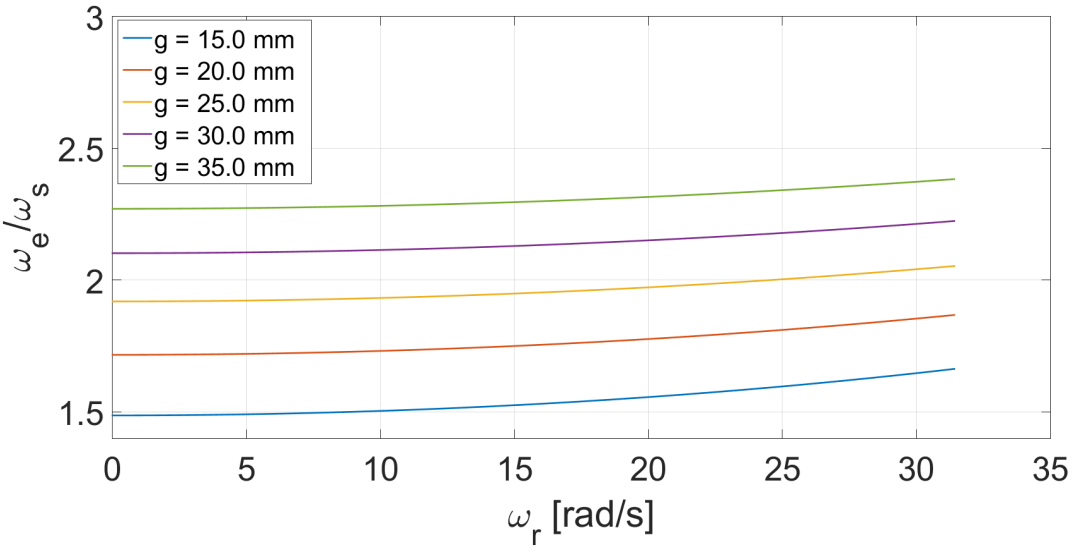

Figure 5.20: ω_e for a low speed motor.

For low speed motors, it must be noted that ω_e can be larger than ω_s [1]. A simulation has been performed in order to prove this, and can be seen in figure 5.20, in which a frequency of 10 Hz was chosen. Again, the phasor corresponding to $\mathbf{B_1}$ is changing its phase over the θ coordinate, but moves in the opposite direction due to a higher speed in relation to $\mathbf{B_s}$ and $\mathbf{j_1}$. Therefore, it can be considered that, for low speed motors, wave $\mathbf{B_1}$ moves counter-clockwise, as seen in figure 5.18.

This phasor analysis serves the purpose of providing an explanation to the different thrust curves obtained in section 5.3. For a typical cylindrical rotary induction motor, it

is expected that, at $s = 0$, thrust is zero. This is to the fact that the thrust is calculated as the cross product between the primary current density and the total magnetic field in the air gap, as per equation 5.5 [1]. If $\mathbf{j_1}$ and $\mathbf{B}$ are in quadrature, then thrust is zero. At a slip of $s = 0$, as previously mentioned, $\delta_s = -\frac{\pi}{2}$, obtained from equation 4.11. However, wave $\mathbf{B_1}$ also exists, as well as wave $\mathbf{B_2}$ which we are neglecting due to its little impact. Therefore, at $s = 0$, the total magnetic field inside the air gap, which is approximately the sum of waves $\mathbf{B_s}$ and $\mathbf{B_1}$, may not be in quadrature with $\mathbf{j_1}$, hence generating a non null thrust at zero slip. In fact, it is possible that null thrust is obtained for a slip lower than zero.

For high speed motors, for small slips, the speed ω_r is close to ω_s, and hence wave $\mathbf{B_1}$ can be considered stationary, and since wave $\mathbf{B_1}$ is in the right plane, thrust generation between itself and $\mathbf{j_1}$ is negative. Therefore, wave $\mathbf{B_1}$ generates a substantial amount of negative thrust, which heavily reduces the total thrust in the small slip region. As the slip increases, motor speed ω_r becomes lower than the synchronous speed ω_s. Therefore, the phasor that represents $\mathbf{B_1}$ starts moving. As it moves clockwise, it changes planes from the left side to the right side, and it remains to do so. Therefore, thrust generated by $\mathbf{B_1}$ and $\mathbf{j_1}$ oscillates from positive to negative, which is represented by the oscillation in thrust curve for high slips, seen in figure 5.17.

For the case of low speed motors, in the high slip region, wave $\mathbf{B_1}$ moves counterclockwise, suggesting the same behaviour as for high speed motors in high slip, explained previously. However, because in low speed region the penetration depth α_1 is very small, as per figures 5.1, 5.4, 5.7 and 5.10, the wave $\mathbf{B_1}$'s amplitude becomes very small, not being possible to observe the oscillatory effect previously mentioned. In the low slip region, because wave's $\mathbf{B_1}$ phasor is located in the right half plane, thrust generation is positive. However, it soon reaches the left half plane, generating negative thrust for slips slightly higher than zero. This effect is very evident in figure 5.16.

5.3.2 Number of Pair-Poles

The number of pair-poles has an influence on motor thrust, such that larger number of pair-poles increases thrust throughput. This is to be expected, when the thrust due to the end effects F_1 in equation B is considered. If k is very large, F_1 becomes zero, hence the overall thrust is essentially given by F_n as the thrust curve without end effects considered.

5.3.3 Secondary resistance value

Remembering that the wave $\mathbf{B_1}$ has the most important role in the air gap's magnetic field, one wishes to reduce its influence. Therefore, reducing the value of α_1 is paramount to this end. Equation 4.31 dictates essentially the $\mathbf{B_1}$ wave's influence on the overall magnetic field inside the air gap, as a measure of penetration of the air gap length. Hence, the value of α_1 must be as low as possible in order to reduce the length of air gap in which wave $\mathbf{B_1}$ can exist. In order to accomplish this, the secondary resistance ρ_s must be as high as possible. In practice, this is not recommended, as higher secondary resistances often require a very thin sheet, which is mechanically fragile.

5.3.4 Air Gap

Again, considering equation 4.31, an increase in the air gap g will reduce the end effect's influence on the motor's performance, as already analysed in section 5.1.1. However, increasing the air gap is not recommended, as it decreases power factor and reduces efficiency [1].

5.3.5 Power Supply Frequency

Influence of the supply's frequency on the penetration depth α_1 is not obvious, as the term ω in equation 4.31 is under the real part of the squared complex number. It is only possible to analyse its influence on α_1 through figure 5.10. It becomes clear that

a higher frequency reduces α_1. However, increasing the frequency also decreases the motor's normal performance by increasing impedances.

Overall, a compromise must be made in order to reduce the influence of the end effects, as most of the parameters that can influence α_1 will also negatively impact the motor performance in some other area.

Chapter 6

Results

This chapter will use the analytical model for the magnetic field inside the air gap obtained in chapter 4 and compare it with simulations from a Finite Element Analysis software.

6.1 Amplitude of the Travelling Wave

As explained in section 4.2.1, if the rotor is fully enclosed by the stator, as a typical rotary machine, a travelling wave with a certain amplitude would be obtained inside the air gap, given by equation 4.11. As such, some simulations were performed in order to verify the validity of the obtained expression, as it can be a good measure for how well the steady-state solution is corresponding to the real values.

For a series of slips, the amplitude of the travelling wave was measured and compared with the Finite Element Analysis software for a fully enclosed rotor geometry. All the motor's parameters are the same as the ones provided in table 5.1. The results can be seen in figures 6.1, 6.2 and 6.3.

Note that some transient terms appear during the Finite Element Analysis simulation which are not present in this work's model simulation. However, it should be clear that only the average value is of use, since if the rotor is fully enclosed by the stator, no end effects should appear. Therefore, the Finite Element Analysis simulation software

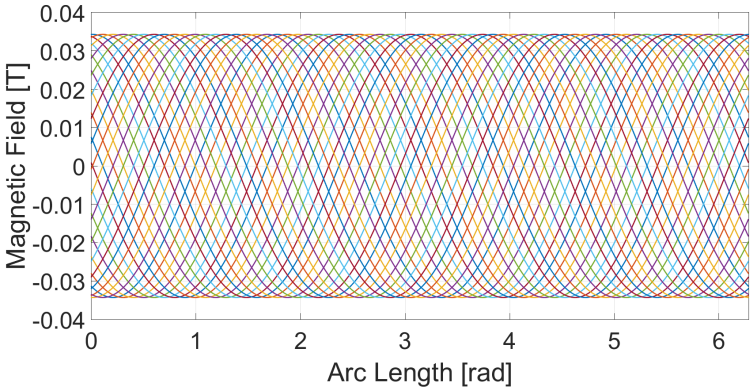

(a) Model simulation.

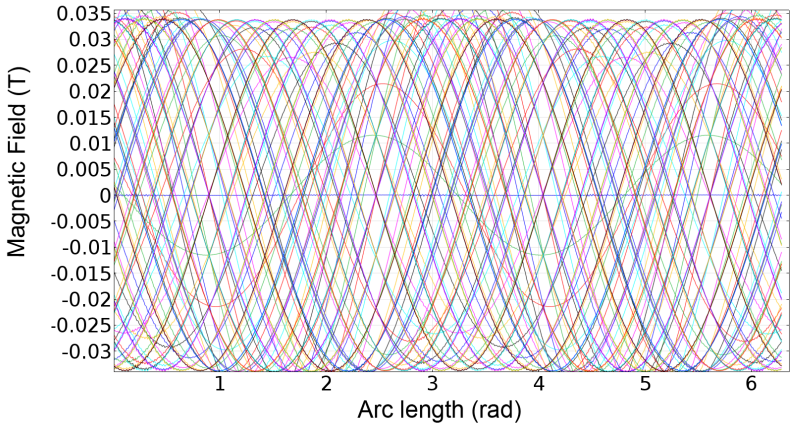

(b) Finite Element Analysis software simulation.

Figure 6.1: $\mathbf{B_s}$ wave simulations for $s = 1$

suffers from some glitches which cannot be fully explained and are considered simply transient terms.

As expected, the expression 4.11 appears to be correct, and in fact holds true for every slip. Also, as expected, with decreasing slip, the travelling wave's amplitude decreases, as less induced current exists in the surface of the secondary. For $s = 1$, this induced current is at its maximum, creating a magnetic field that opposes the one created by the primary current density, therefore reducing the overall magnetic field inside the air gap. For $s = 0$ the opposite effect occurs, as the induced current is at its minimum, creating very little opposing magnetic field.

For better readability, table 6.1 was composed summarizing the results obtained in

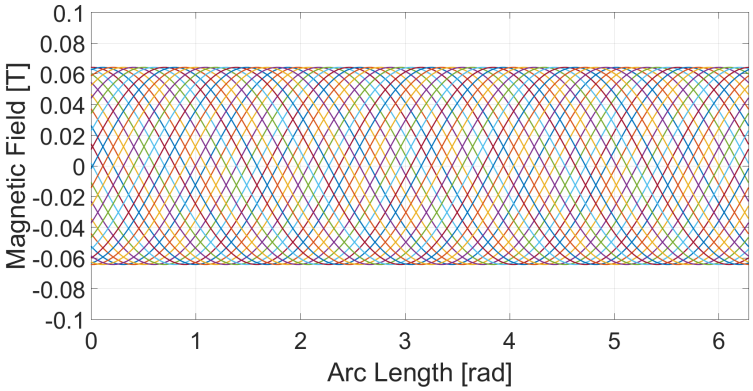

(a) Model simulation.

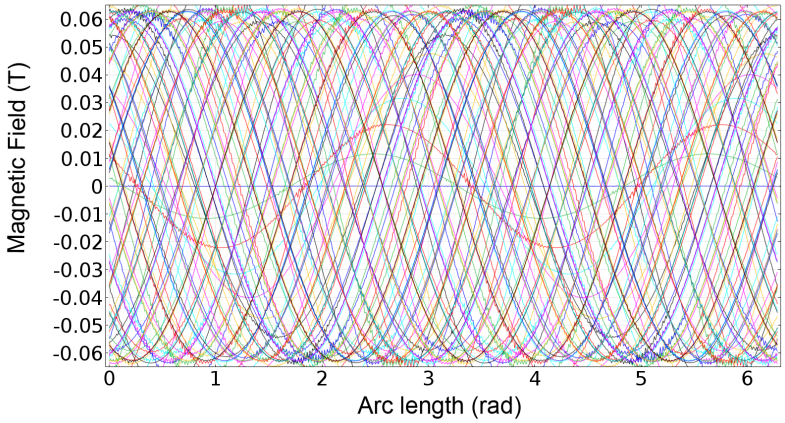

(b) Finite Element Analysis software simulation.

Figure 6.2: $\mathbf{B_s}$ wave simulations for $s = 0.5$

figures 6.1, 6.2 and 6.3.

It must be noted that, as already explained in section 4.2.5, the proposed model only handles the magnetic field inside the air gap. Therefore, it cannot calculate magnetic field outside of it. This is of course not a limitation for the Finite Element Analysis software, which will therefore plot the magnetic field inside the air gap as well as outside. Hence, for the following plots, only the arc length corresponding to $\beta = \pi$ should be considered, or rather, the arc length corresponding to the stator angle, as it is in this zone that the air gap exists, and it will be this zone that the proposed model will simulate.

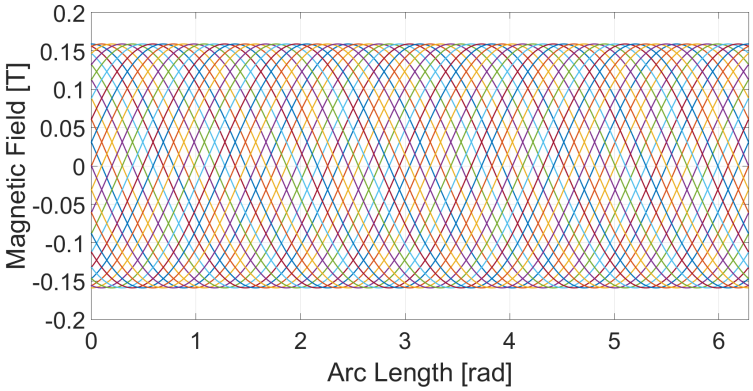

(a) Model simulation.

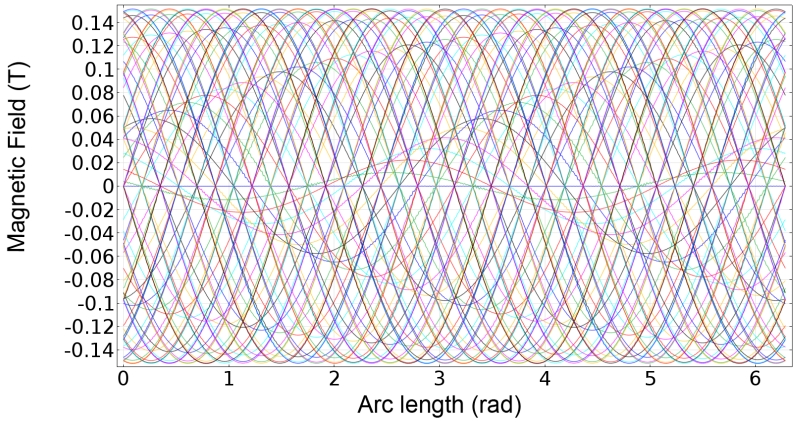

(b) Finite Element Analysis software simulation.

Figure 6.3: $\mathbf{B_s}$ wave simulations for $s = 0$

6.2 Total Magnetic Field inside the Air Gap

The total magnetic field inside the air gap is given by the expression 4.36. In section 6.1, the $\mathbf{B_s}$ wave was studied and the model proposed was verified as an accurate representation of the actual travelling wave inside the air gap. Now, waves $\mathbf{B_1}$ and $\mathbf{B_2}$ will be added, corresponding to the actual end effects.

6.2.1 Finite Element Analysis Software Simulations

Using a Finite Element Analysis software, a model sharing the same geometric characteristics as the ones in table 5.1 was created and simulated for various slips over

Slip	$s = 1$	$s = 0.5$	$s = 0$
Finite Element Analysis Software (T)	0.034	0.062	0.149
One dimensional model (T)	0.034	0.064	0.159

Table 6.1: Travelling wave's magnetic field amplitude obtained in the Finite Element Analysis software and through simulation of the proposed model.

time. The resulting magnetic field inside the air gap was obtained, and is shown in figures 6.4, 6.5, 6.6 and 6.7.

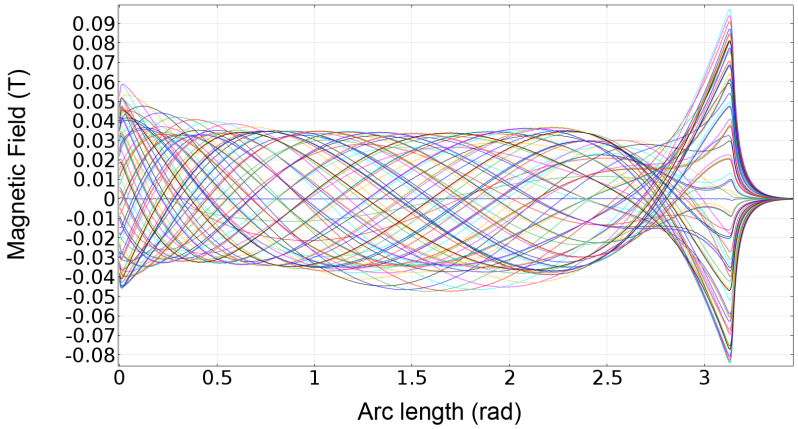

Figure 6.4: Finite Element Analysis simulation for $s = 1$.

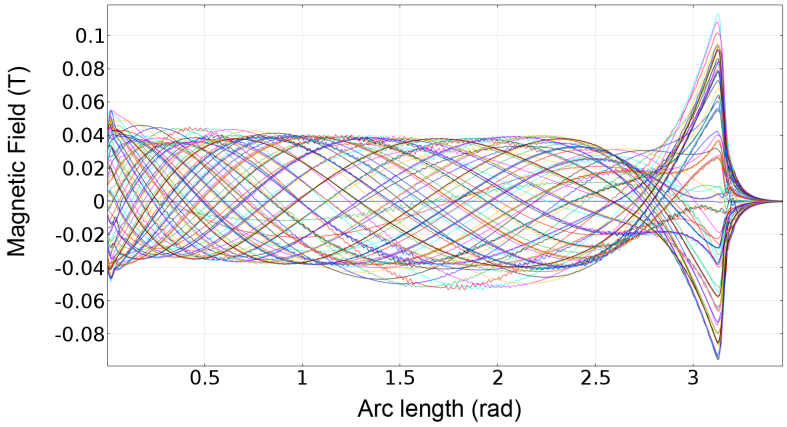

Figure 6.5: Finite Element Analysis simulation for $s = 0.9$.

Already, it can be seen that the magnetic field does indeed have a complicated

profile inside the air gap, which can only be somewhat explained through the analysis made in chapter 1. For high slips, for most of the air gap, the magnetic field seems to be close to the travelling wave alone, except for near the extremities of the motor. In the entry end, which is on the left side of the figures, magnetic field seems to increase. This however does not go against the theory provided in chapter 1 regarding the dynamic end effects, since for high slip, the motor can be considered stationary, under little effect of the dynamic end effects and as such were not included in that analysis. However, it can be explained as the amplitude of wave $\mathbf{B_1}$ being larger than the amplitude of wave $\mathbf{B_S}$ for high slips. The obtained expression for $\mathbf{B_1}$, in appendix A, is too complex to be analysed in such a way, and as such this will be discussed quantitatively in the next section.

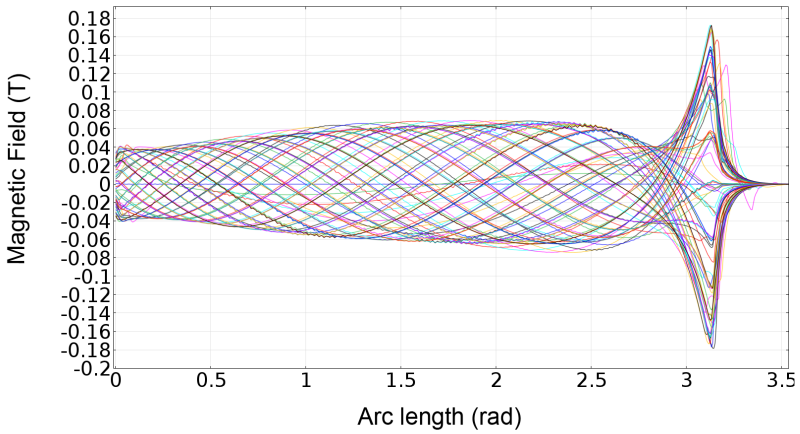

Figure 6.6: Finite Element Analysis simulation for $s = 0.5$.

Another interesting note for analysis is the funneling of magnetic field that seems to occur for any slip, near the exit end, corresponding to the right side of the figures. This point can be explained if the two waves that make up the proposed model are remembered, as one travel in one direction and the other in the opposite direction, which different attenuation constants. This funnel point is where the exit end effect wave starts influencing the magnetic field. Since its damping constant is very small, its impact is reduced to a very limited arc length near the exit, therefore creating a very sudden increase in the magnetic field.

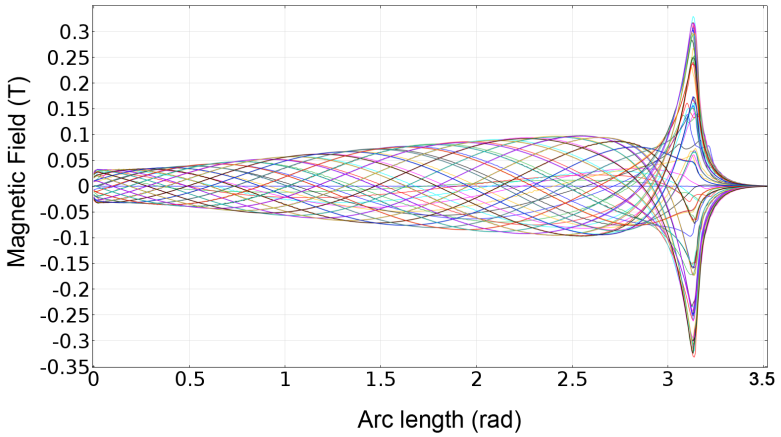

Figure 6.7: Finite Element Analysis simulation for $s = 0.1$.

For low slips the magnetic field seems to correspond almost exactly to what was expected in theory. In the entry end, a reduced magnetic field is obtained, while near the exit end it is increased substantially.

6.2.2 First set of Boundary Conditions

Using the first set of simple boundary conditions, where the flux conservation is calculated between $\theta = 0$ and $\theta = \beta = \pi$, plots were made, for various slips, and can be seen in figures 6.8, 6.9, 6.10 and 6.11.

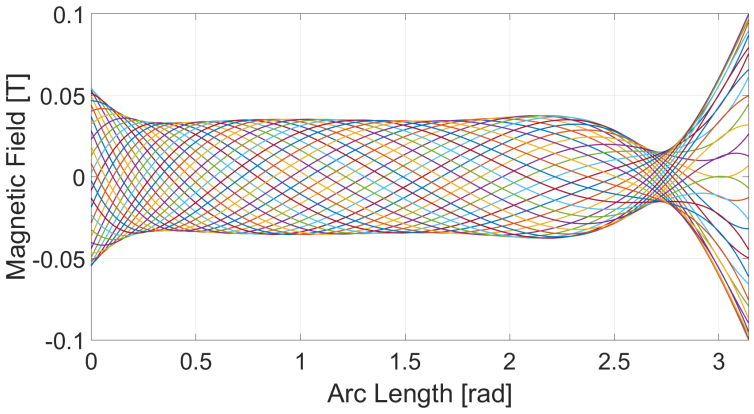

Figure 6.8: Model simulation for $s = 1$ with simple boundary conditions.

The individual waves' amplitudes are shown in table 6.2, following figures 5.13, 5.14

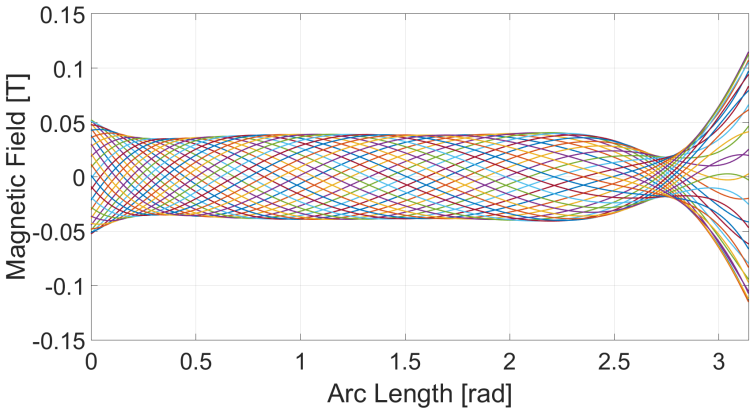

Figure 6.9: Model simulation for $s = 0.9$ with simple boundary conditions.

and 5.15.

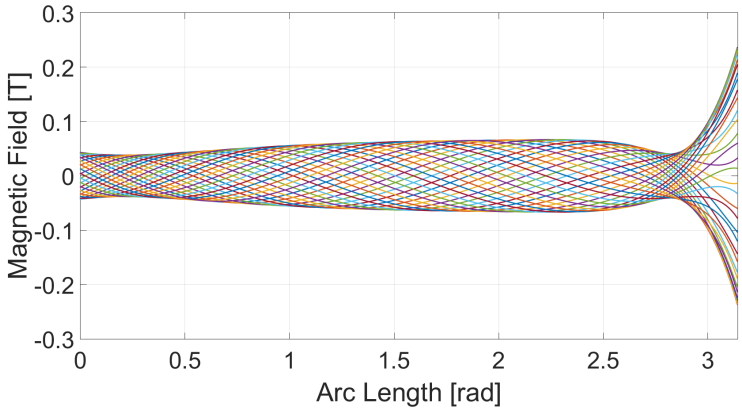

Figure 6.10: Model simulation for $s = 0.5$ with simple boundary conditions.

Slip	$s = 1$	$s = 0.9$	$s = 0.5$	$s = 0.1$
Travelling wave $\mathbf{B_S}$ (T)	0.0343	0.0379	0.0643	0.1448
Entry wave $\mathbf{B_1}$ (T)	0.0730	0.0748	0.0924	0.1483
Exit wave $\mathbf{B_2}$ (T)	0.0544	0.0651	0.1460	0.3661

Table 6.2: Amplitudes for each wave as described by the one dimensional model for simulated slips.

For high slips, the model for the magnetic field inside the air gap with the first set of boundary conditions seems to represent accurately the actual magnetic field, as it is in accordance with the Finite Element Analysis software. For lower slips, however,

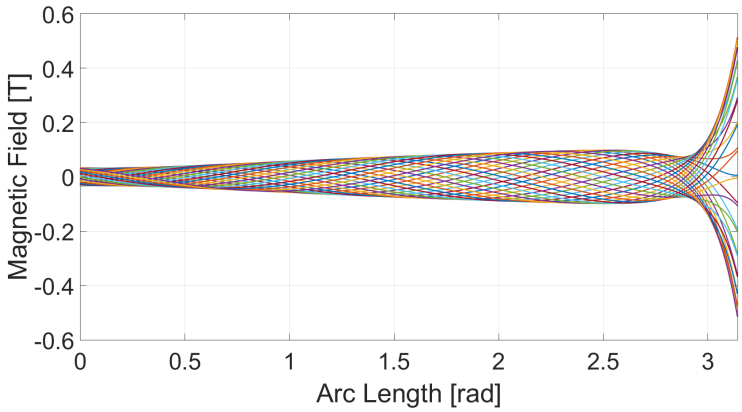

Figure 6.11: Model simulation for $s = 0.1$ with simple boundary conditions.

it seems that near the exit end of the air gap, where the $\mathbf{B_2}$ wave exists, the model is overestimating the impact of the $\mathbf{B_2}$ wave, and as such, the magnetic field peak near the end does not coincide with the FEA software. One reason for this may be the over-simplistic boundary conditions considered for the calculation of amplitudes $\mathbf{B_1}$ and $\mathbf{B_2}$. As is evident in the previous plots, the Finite Element Analysis software is capable of calculating the magnetic field outside the air gap, forcing it to decrease exponentially to zero. This is not predicted in these boundary conditions, as they only handle the magnetic field inside the actual air gap. Therefore, the flux conservation still holds true, but has to be considered for a larger length than just the actual stator length β, as explained in the second set of boundary conditions in section 4.2.5. As such, these boundary conditions are considering the same amount of magnetic flux than the Finite Element Analysis software but over a shorter θ coordinate angle, which will affect the wave's amplitudes. In fact, the $\mathbf{B_2}$ was calculated with the conservation of the magnetic flux as per equation 4.40, and as such, is the only amplitude affected by the mismatch of the magnetic flux, which explains why only near the exit these boundary conditions seem to differ from the Finite Element Analysis software.

However, taking into account that the $\mathbf{B_2}$ wave exists in a very limited zone near the exit end of the motor, this set of simple boundary conditions can produce an accurate profile for the magnetic field inside the air gap for most of its length.

6.2.3 Second set of Boundary Conditions

A value for ξ must be estimated, according to the second set of boundary conditions proposed. Various simulations were tested and the value that seemed to result in a closer profile to the Finite Element Analysis software was $\xi = 0.0483$. Note that this value for ξ should only be used as an approximation for these motor specifications, as per table 5.1.

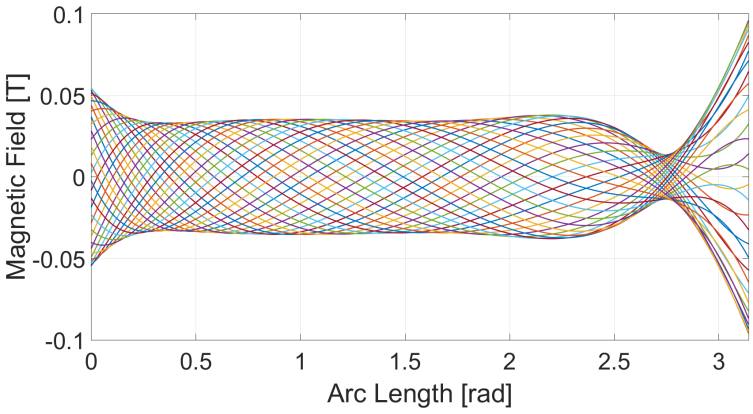

Figure 6.12: Model simulation for $s = 1$ with second set of boundary conditions.

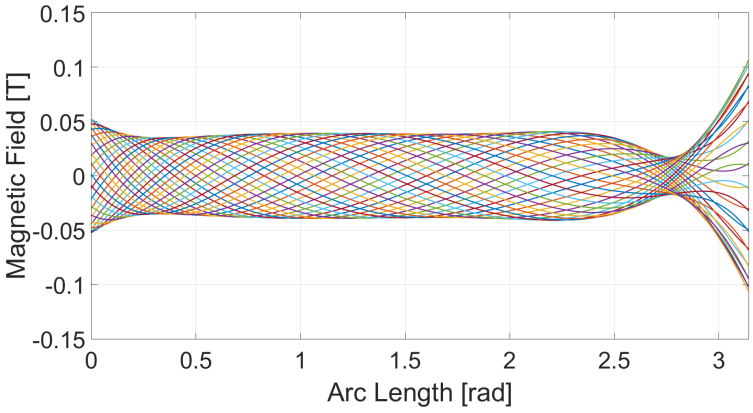

Figure 6.13: Model simulation for $s = 0.9$ with second set of boundary conditions.

For high slips, comparing figures 6.12 and 6.13 to figures 6.4 and 6.5, it seems that the new boundary conditions accurately describe the magnetic field profile, and don't deviate much from the results obtained from the simpler boundary conditions. It is for lower slips, and hence higher motor speeds, that the new set of boundary conditions

will provide better results for the magnetic field.

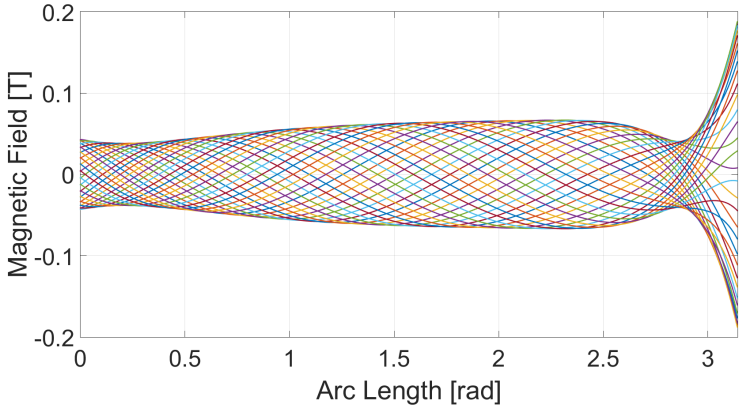

Figure 6.14: Model simulation for $s = 0.5$ with second set of boundary conditions.

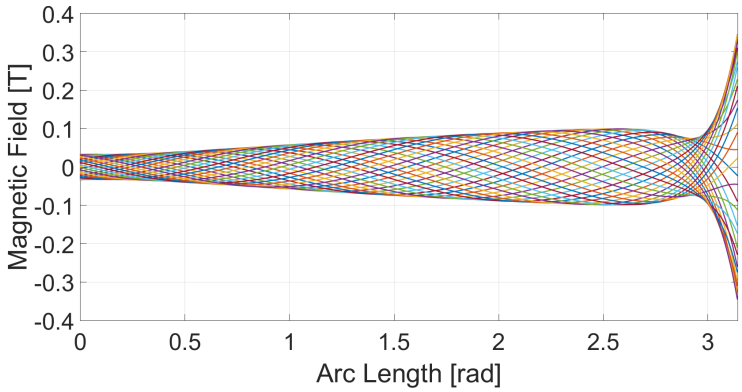

Figure 6.15: Model simulation for $s = 0.1$ with second set of boundary conditions.

Frequency f	20 Hz
Number of pole-pairs k	2
Primary sheet width d_s	2 mm
Secondary sheet width d_r	2 mm
Rotor radius r_r	70 mm
Air gap length g	2 mm
Stator angle β	π rad
Secondary sheet resistivity ρ_s	1.0x10^{-5} Ω
Primary current density J_M	1x10^6 A/m

Table 6.3: Motor parameters used for model's parameters' plots.

As observed in figures 6.14 and 6.15, compared to 6.6 and 6.7, there is a high degree of similarity. The new boundary conditions provide a very accurate representation of the magnetic field inside the air gap for all slips.

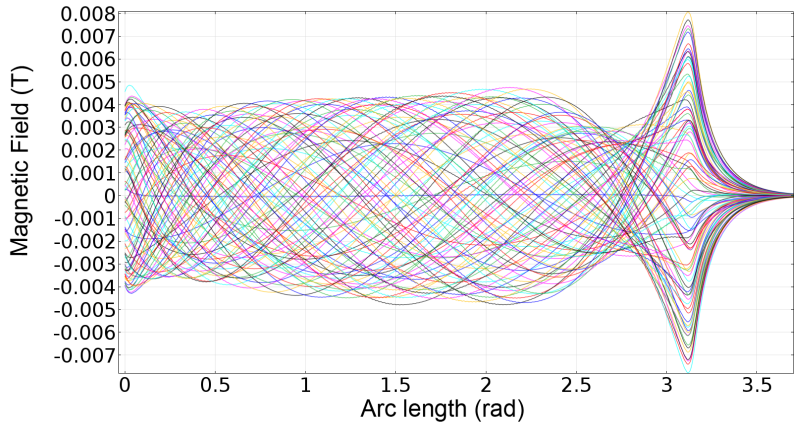

(a) Finite Element Analysis software.

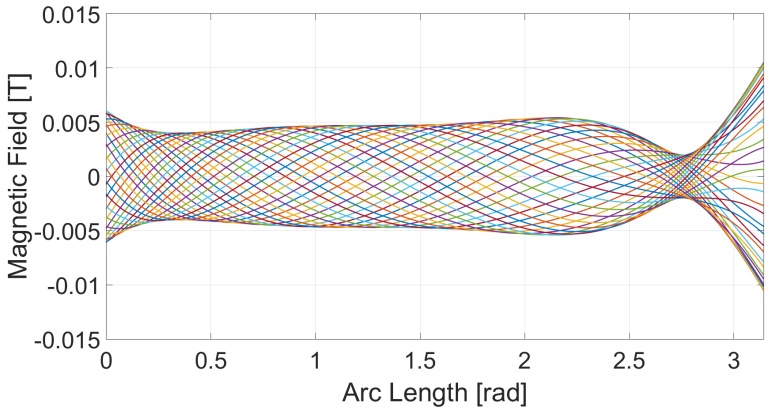

(b) Proposed model.

Figure 6.16: Simulations for second motor for $s = 1$.

Having solved the accuracy problem for the low slip regions, the second set of boundary conditions can be applied to fully describe the profile of the magnetic field inside the air gap for any motor parameters, remaining inside the initial assumptions such as small air gap. The ξ parameter, however, is chosen somewhat arbitrarily and should depend on the motor's parameters.

A different motor is then imagined, following table 6.3. The second set of boundary

conditions will be applied to this new motor with different physical properties, in order to make sure that the results obtained previously do not suffer from over fitting the model to that specific motor. The new value used was $\xi = 0.1571$.

The results for this new motor are shown in figures 6.16, 6.17, 6.18 and 6.19. The simulation made through the Finite Element Analysis software and the simulation of the proposed model can be seen side by side. Even for these new motor characteristics, the second set of boundary conditions describe with high accuracy the profile of the magnetic field inside the air gap.

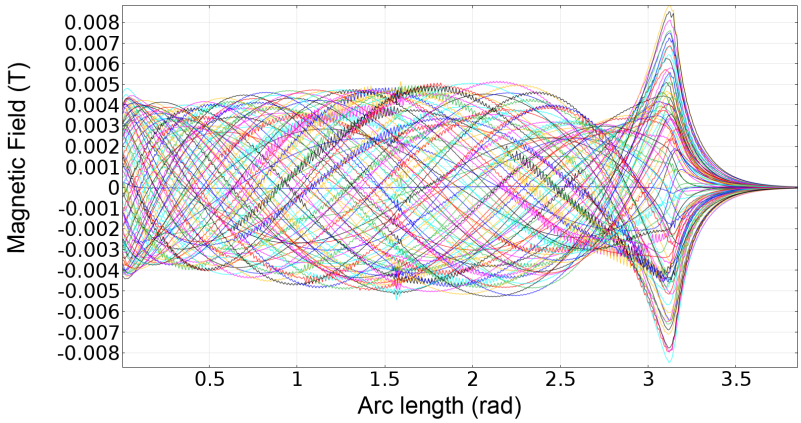

(a) Finite Element Analysis software.

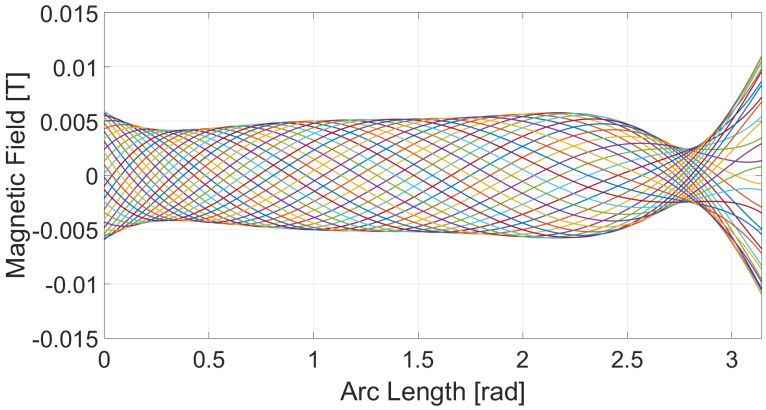

(b) Proposed model.

Figure 6.17: Simulations for second motor for $s = 0.9$.

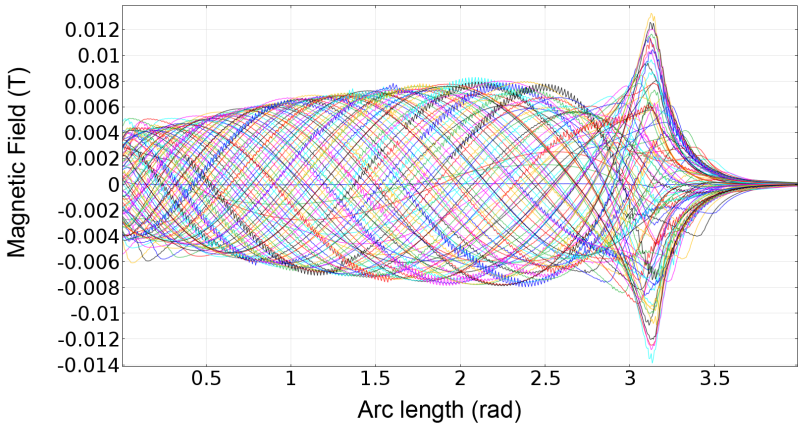

(a) Finite Element Analysis software.

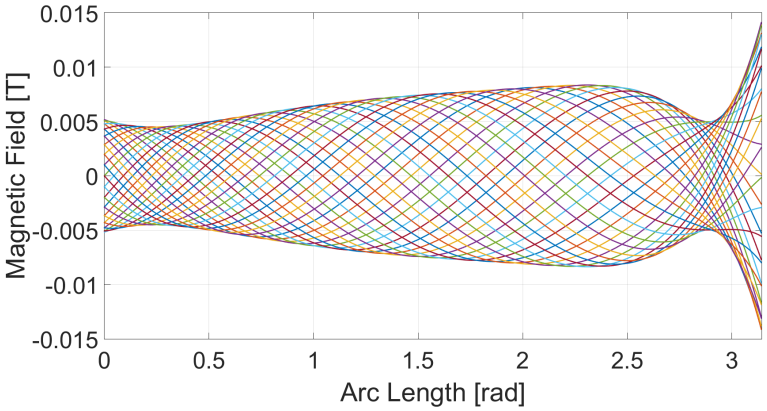

(b) Proposed model.

Figure 6.18: Simulations for second motor for $s = 0.5$.

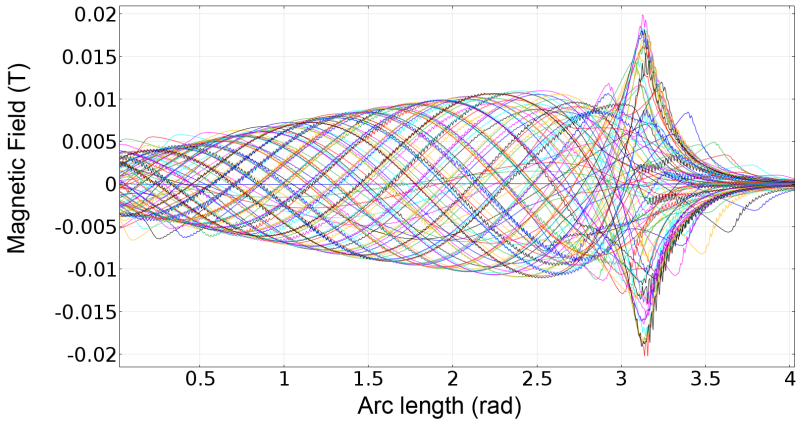

(a) Finite Element Analysis software.

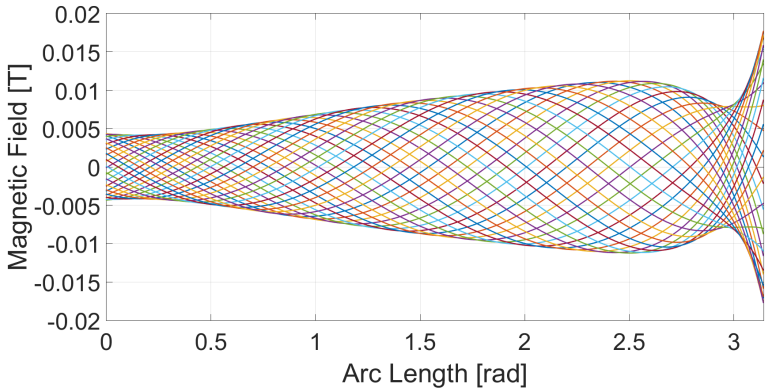

(b) Proposed model.

Figure 6.19: Simulations for second motor for $s = 0.1$.

6.2.4 Other stator angles

In the previous sections, all simulations were made with $\beta = \pi$, for simplicity and comparability's sake. As referred in section 5.1.5, β should be limited to 2π, since the model will not handle $\beta > 2\pi$ correctly.

Other β were chosen, namely $\frac{\pi}{2}$ and $\frac{2\pi}{3}$, based on the motor parameters of table 5.1 with frequency $f = 10Hz$. Two slips were chosen, as to demonstrate the behaviour of the motor in high and low speed regions: $s = 0.05$ and $s = 0.7$. The second set of boundary conditions were applied to the proposed model. The following figures 6.20, 6.21 show the Finite Element Analysis software output and the proposed

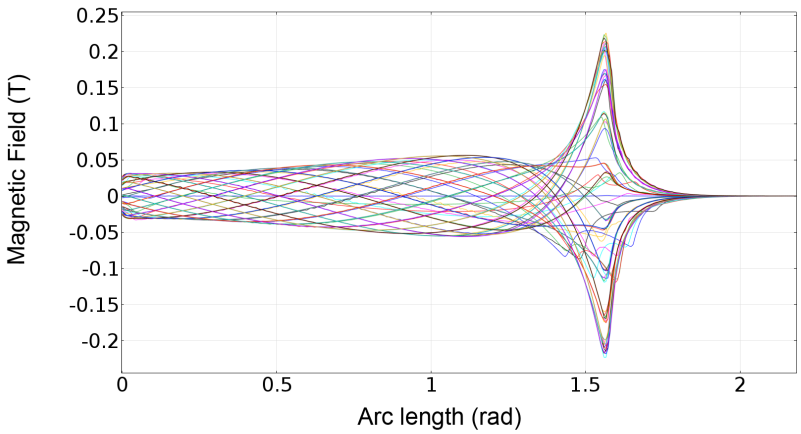

(a) Finite Element Analysis software.

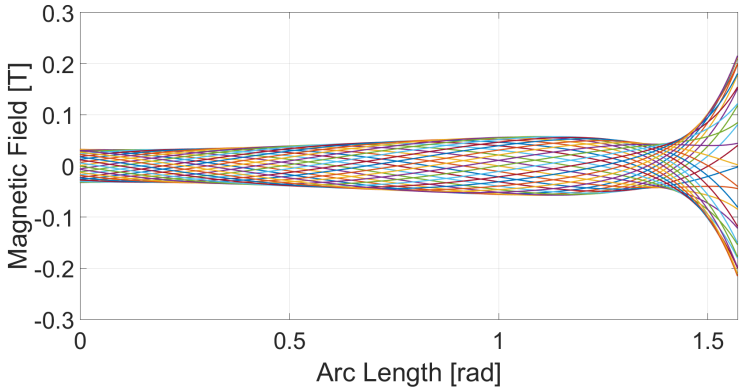

(b) Proposed model.

Figure 6.20: Simulations for $\beta = \frac{\pi}{2}$ and $s = 0.05$.

model's output for $\beta = \frac{\pi}{2}$. The chosen value of ξ was the same as used in the previous section 6.2.3, suggesting that ξ does not depend on the stator angle β but rather on the other physical properties of the motor, such as rotor radius and air gap length.

The proposed model once again seems to describe the phenomenon of the end effects accurately, even for other stator angles, suggesting that the second set of boundary conditions does indeed solve the problem of the leakage magnetic flux that is not taken being taken into account.

Results for $\beta = \frac{3\pi}{2}$ are shown in figures 6.22 and 6.23.

Even for large stator angles the model with the second set of boundary conditions explains the profile of the magnetic field inside the air gap. These results validate the

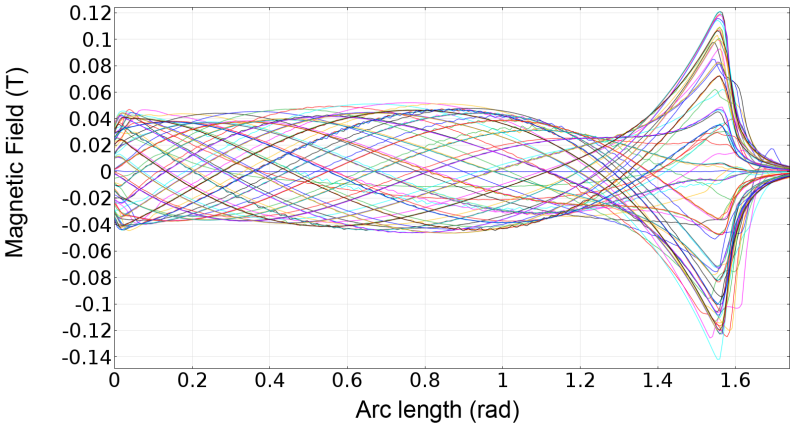

(a) Finite Element Analysis software.

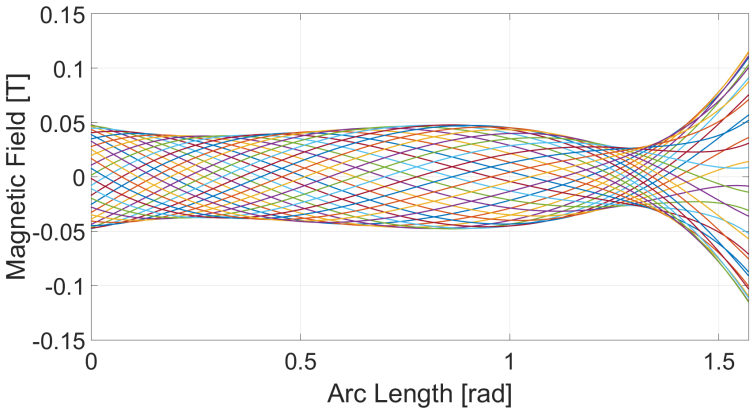

(b) Proposed model.

Figure 6.21: Simulations for $\beta = \frac{\pi}{2}$ and $s = 0.7$.

proposed model which can however be improved upon.

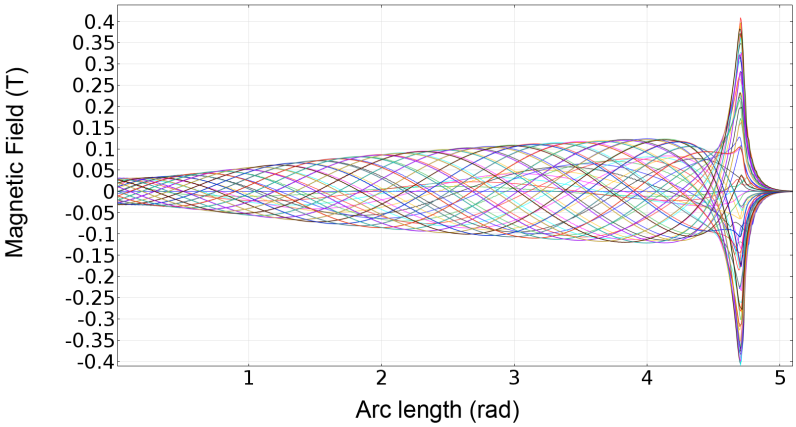

(a) Finite Element Analysis software.

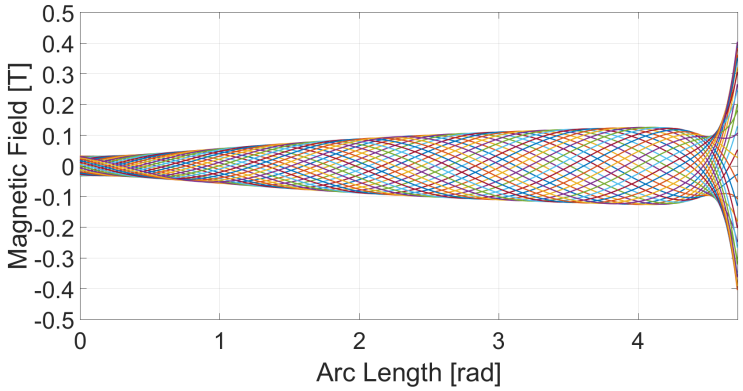

(b) Proposed model.

Figure 6.22: Simulations for $\beta = \frac{3\pi}{2}$ and $s = 0.05$.

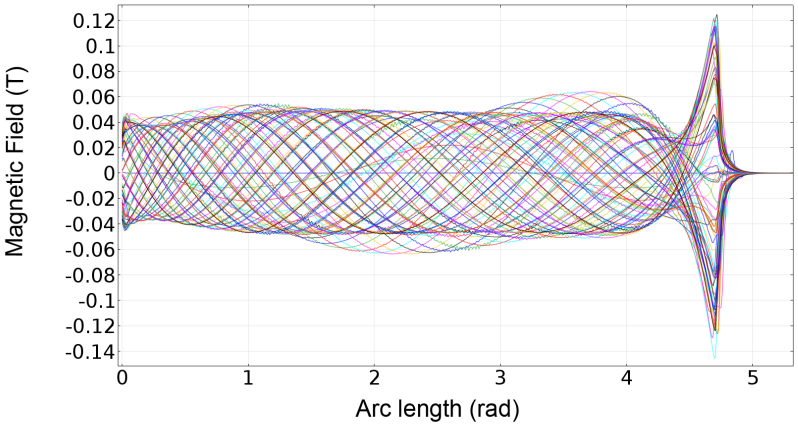

(a) Finite Element Analysis software.

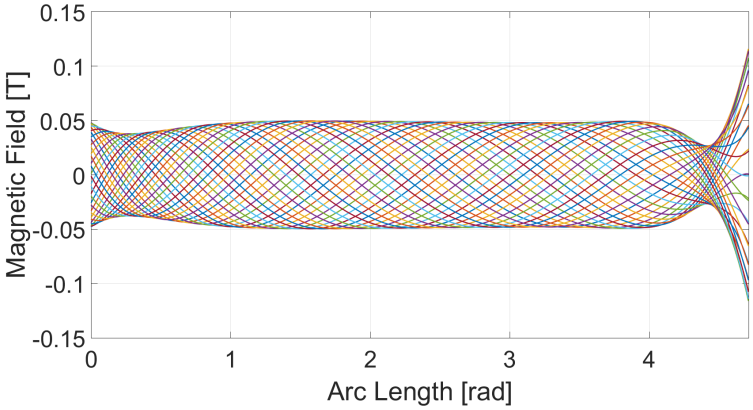

(b) Proposed model.

Figure 6.23: Simulations for $\beta = \frac{3\pi}{2}$ and $s = 0.7$.

Chapter 7

Conclusions

This work proposes a one dimensional model based on the Field Theory to describe the magnetic field inside a spherical induction motor with shell-like stator. The model uses the as basis the linear induction motor models for end effects, and it accurately corresponds to simulations produced by the Finite Element Analysis software. The motor's properties on the model's parameters were studied and can serve as a basis for design of this type of motor, in order to reduce the effect of the end effects on motor performance.

In chapter 4, the one dimensional model was presented through analysis of the electromagnetic laws. Some approximations were made, including the non variation of the magnetic field in the θ coordinate, a small air gap and equivalent conductive sheets for the primary winding and the secondary sheet. These approximations are based on previous work in linear induction motors' analysis through Field Theory, such as in references [1] and [5]. The resulting model produces two end effects waves, $\mathbf{B_1}$ and $\mathbf{B_2}$, which can be thought of as the entry end effect wave and the exit end effect wave, correspondingly, which, in conjunction with the travelling wave $\mathbf{B_S}$ translate the profile of the magnetic field inside the air gap. These end effect waves travel in opposite directions in terms of the θ coordinate, and have different damping constants α_1 and α_2.

The biggest problem concerning the model itself was the definition of the boundary

conditions, where two sets of boundary conditions were defined. The first set is a very simplistic approach, where it is considered that outside the air gap there is no magnetic flux or induced currents. As the results showed in chapter 6, these simplistic conditions do not produce a good enough result for the profile of the magnetic field inside the air gap. Therefore, a second set of boundary conditions had to be found, where a small angle ξ outside of the air gap was considered, in which magnetic field and induced currents could exist. This ξ angle is arbitrary, and only with the help of the Finite Element Analysis software results was it possible to estimate a value for it. After achieving a value that corresponded to the Finite Element Analysis software, all the simulations made with the same ξ seemed to correspond to the Finite Element Analysis software simulations.

The obtained parameters of the model were discussed and their sensitivity to the motor physical properties was analysed in chapter 5. Some interesting points were made, specifically regarding the difference between high speed and low speed motors, as the model's parameters seem to have a complete opposite behaviour from a certain undefined point in terms of motor speed. This undefined point, or rather undefined area, can be estimated through the γ parameter found, which depends on the motor's physical properties such as radius and secondary sheet conductivity. The biggest conclusion in this section is the difference between the penetration depths α_1 and α_2, which defined the damping of the end effect waves as they travel through the θ coordinate. It was found that α_1 is generally much larger than α_2, hence wave $\mathbf{B_1}$ should have a much larger contribution of the distortion of the magnetic field inside the air gap than wave $\mathbf{B_2}$. This corresponds to the previous work done on the linear induction motor as well.

Lastly, various simulations were made in the Finite Element Analysis software in order to validate the proposed model. Three stator angles were chosen and various different slips were used. The first set of boundary conditions can explain the larger part of the profile of the magnetic field inside the air gap, but its results near the entry and exit ends specifically are not validated by the Finite Element Analysis software. The second set of boundary conditions however seem to be in total accordance to the

Finite Element Analysis software, particularly in the entry and exit ends of the motor.

The model, when the second set of boundary conditions are used, explains the complicated profile of magnetic field found inside the air gap.

The one dimensional model is a very simplified model which proved to be a good representation of the motor's behaviour. However, the model should not be used for very large air gaps, as one of the initial assumptions was a small air gap. This will introduce almost certainly a variation of the magnetic field in the θ coordinate, which is not considered at all in the one dimensional model. Therefore, a two dimensional model could be designed, following the work already done on that subject regarding linear induction motors by [1] and [5].

A new set of equations could be considered for the one dimensional model in order to describe the magnetic field inside the air gap as well as outside the air gap, even if just in the vicinity. This, in conjunction with better boundary conditions, could enhance the model's accuracy tenfold. Work on this subject has been done primarily by [5], creating one dimensional models of second, third and fourth order.

A more extensive work on the influence of motor parameters on motor performance can be done, namely the impact on power, efficiency and torque. For this, models such as the equivalent circuit proposed by [9] could be used.

Bibliography

[1] Sake Yamamura. *Theory of Linear Induction Motors*. Halsted, 1972. ISBN: 0-470-97090-1.

[2] E. Amiri, E. Mendrela. *Induction Motors with Rotor Helical Motion*. InTech, 2012. ISBN: 978-953-0843-6.

[3] H. Tiegna, Y. Amara, G. Barakat. Overview of analytical models of permanent magnet electrical machines for analysis and design purposes. *Elsevier B.V*, 2013.

[4] B. Bessaih, A. Boucheta, I. K. Bousserhane, A. Hazzab. Speed control of linear induction motor considering end-effects compensation using rotor time constant estimation. *9th International Multi-Conference on Systems, Signal and Devices*, 2012.

[5] Michel Poloujadoff. *The Theory of Linear Induction Machinery*. Clarendon, 1972. ISBN: 0-19-959322-8.

[6] Ion Boldea, S. A. Nasar. *Linear Motor Electromagnetic Devices*. Taylor and Francis, 2001. ISBN: 90-5699-702-5.

[7] A. Accetta, M. Pucci, A. Lidozzi, L. Solero, F. Crescimbini. Compensation of static end effects in linear induction motor drives by frequency-adaptive synchronous controllers. *International Conference on Electrical Machines (ICEM)*, 2014.

[8] Ion Boldea. *Linear Electric Machines, Drives, and MAGLEVs Handbook*. Taylor and Francis, 2013. ISBN: 978-1-4398-4515-8.

[9] J. Duncan. Linear induction motor-equivalent-circuit model. *IEEE Transactions on Industrial Electronics*, 1983.

[10] João F. P. Fernandes, P. J. Costa Branco. The shell-like spherical induction motor for low-speed traction: Electromagnetic design, analysis and experimental tests. *IEEE Transactions on Industrial Electronics*, 2015.

[11] Klemens Kahlen. Torque control of a spherical machine with variable pole pitch. *IEEE Transactions on Power Electronics*, 2004.

[12] Carlos Manuel Pereira Cabrita. *Motor Linear de Indução - Análise Teórica, Projecto e Ensaio*. PhD thesis, Instituto Superior Técnico, 1988.

[13] J. Gieras. *Linear Induction Drives*. Clarendon, 1994. ISBN: 0-19-8593-813.

[14] E. Mendrela. *Modeling of Induction Motors with One and Two Degrees of Mechanical Freedom*. Clarendon, 1994. ISBN: 0-19-8593-813.

[15] E. Fernandes da Silva, E. Bueno dos Stanso, Paulo C. M. Machado, Marco A. A. de Oliveira. Dynamic model for linear induction motors. *IEEE ICIT*, 2003.

[16] J. F. Gieras, G. E. Dawson, A. R. Eastham. A new longitudinal end effect factor for linear induction motors. *IEEE Transactions on Energy Conversion*, 1987.

[17] Wei Xu. Equivalent circuit derivation and performance analysis of a single-sided linear induction motor based on the winding function theory. *IEEE Transactions on Vehicular Technology*, 1987.

[18] Nobuo Fujii, Toshiyuki Harada, Yasuaki Sakamoto, Takeshi Kayasuga. A compensation method for the end effect of a linear induction motor. *Denki Gakkai Ronbunshi*, 2002.

[19] Xiaozhou Guo, Bin Zhou, Jisan Lian. A new method to reduce end effect of linear induction motor. *Journal of Modern Transportation*, 2012.

[20] A. J. Sinistera. *Modeling of Linear Induction Machines for Analysis and Control*. Clarendon, 1994. ISBN: 0-19-8593-813.

Appendix A

Expression for wave B_1

As per section 4.2.5, waves $\mathbf{B_1}$ and $\mathbf{B_2}$ have a complex amplitude, $\overline{B_1}$ and $\overline{B_2}$, correspondingly. The amplitude $\overline{B_2}$ has already been calculated, but amplitude $\overline{B_1}$ has not, as the resulting expression is too large to be readable in a easy way. Therefore, the aim of this appendix is to write the exact expression of $\overline{B_1}$ that was used throughout this work, and can be found in equation A.1.

$$\overline{B_1} = -\frac{-J_1(\frac{1}{r_g}+1)}{\frac{\overline{s_1}+\frac{\overline{s_2}^2\exp(-\overline{s_2}\beta)(\exp(\overline{s_1}\beta)-1)}{\overline{s_1}(\exp(-\overline{s_2}\beta)-1)}}{r_g\mu_0} - \frac{r_r\omega_r\frac{\overline{s_2}\exp(-\overline{s_2}\beta)(\exp(\overline{s_1}\beta)-1)}{\overline{s_1}(\exp(-\overline{s_2}\beta)-1)}+1}{\rho_s}} + \frac{\frac{\jmath k\overline{B_S}+\frac{\overline{s_2}^2\exp(-\overline{s_2}\beta)(\jmath\overline{B_S}-\jmath\overline{B_S}\exp(-\jmath k\beta))}{k(\exp(-\overline{s_2}\beta)-1)}}{r_g\mu_0}}{\frac{\overline{s_1}+\frac{\overline{s_2}^2\exp(-\overline{s_2}\beta)(\exp(\overline{s_1}\beta)-1)}{\overline{s_1}(\exp(-\overline{s_2}\beta)-1)}}{r_g\mu_0} - \frac{r_r\omega_r\frac{\overline{s_2}\exp(-\overline{s_2}\beta)(\exp(\overline{s_1}\beta)-1)}{\overline{s_1}(\exp(-\overline{s_2}\beta)-1)}+1}{\rho_s}} + \frac{r_r\omega_r(\overline{B_S}-\frac{\overline{s_2}\exp(-\overline{s_2}\beta)(\jmath\overline{B_S}-\jmath\overline{B_S}\exp(-\jmath k\beta))}{k(\exp(-\overline{s_2}\beta)-1)})}{\rho_s}}{\frac{\overline{s_1}+\frac{\overline{s_2}^2\exp(-\overline{s_2}\beta)(\exp(\overline{s_1}\beta)-1)}{\overline{s_1}(\exp(-\overline{s_2}\beta)-1)}}{r_g\mu_0} - \frac{r_r\omega_r\frac{\overline{s_2}\exp(-\overline{s_2}\beta)(\exp(\overline{s_1}\beta)-1)}{\overline{s_1}(\exp(-\overline{s_2}\beta)-1)}+1}{\rho_s}} \tag{A.1}$$

Appendix B

Expression for Thrust due to wave $\mathbf{B_1}$

The thrust F_1 due to wave $\mathbf{B_1}$ describes the effect of the entry end effect on thrust, when disregarding the effects of wave $\mathbf{B_2}$. Adding to this value the thrust generated by $\mathbf{B_S}$ and the total motor thrust, under end effects, is $F_n + F_1$. The expression for F_1 is presented in this appendix, under equation B.1.

$$
\begin{aligned}
F_1 =& \frac{\alpha_1(\cos(\delta_1) + \alpha_1 k \sin(\delta_1) + \alpha_1 k_e \sin(\delta_1))}{\alpha_1^2 k^2 + 2\alpha_1^2 k k_e + \alpha_1^2 k_e^2 + 1} \\
&- \frac{\alpha_1 exp(-\frac{\beta}{\alpha_1})(\cos(\delta_1 - \beta k - \beta k_e) + \alpha_1 k \sin(\delta_1 - \beta k - \beta k_e) + \alpha_1 k_e \sin(\delta_1 - \beta k - \beta k_e))}{\alpha_1^2 k^2 + 2\alpha_1^2 k k_e + \alpha_1^2 k_e^2 + 1} \\
&+ \frac{\alpha_1(\cos(\delta_1) - \alpha_1 k \sin(\delta_1) + \alpha_1 k_e \sin(\delta_1))}{(\alpha_1^2 k^2 - 2\alpha_1^2 k k_e + \alpha_1^2 k_e^2 + 1)} \\
&- \frac{\alpha_1 exp(-\frac{\beta}{\alpha_1})(\cos(\delta_1 + \beta k - \beta k_e) - \alpha_1 k \sin(\delta_1 + \beta k - \beta k_e) + \alpha_1 k_e \sin(\delta_1 + \beta k - \beta k_e))}{\alpha_1^2 k^2 - 2\alpha_1^2 k k_e + \alpha_1^2 k_e^2 + 1}
\end{aligned}
\tag{B.1}
$$